Spatial and temporal mechanisms of vagus motor neuron topographic map development

Gabrielle R. Barsh

A dissertation

submitted in partial fulfillment of the

requirements for the degree of

Doctor of Philosophy

University of Washington

2017

Reading Committee:

Cecilia Moens, Chair

David Beier

Slobodan Beronja

Program Authorized to Offer Degree:

Molecular & Cellular Biology

University of Washington

Abstract

Spatial and temporal mechanisms of vagus motor neuron topographic map development

Gabrielle R. Barsh

Chair of the Supervisory Committee:

Affiliate Professor Cecilia B. Moens

Division of Basic Sciences, Fred Hutchinson Cancer Research Center

Many networks throughout the nervous system are organized into topographic maps, where the positions of neuron cell bodies in the projecting field correspond with the positions of their axons in the target field. Previous studies of topographic map development show evidence for spatial patterning mechanisms, in which gene expression patterns in the projecting and target fields determine axon targeting in a manner that depends on the precise positions of the cell bodies. Here, we describe a novel mechanism of topographic map formation that depends on the timing of axon outgrowth, and that is overlaid on spatial patterning mechanisms. We focus on the

vagus motor neurons, which are topographically arranged in both mammals and fish. We show that cell position along the anterior-posterior axis of hindbrain rhombomere 8 determines expression of *hox5* genes, which are expressed in posterior vagus motor neurons. Using live-imaging techniques in zebrafish embryos, we additionally reveal a difference in time of axon formation between anterior versus posterior motor neurons that is independent of neuron birth time. We show that *hox5* expression directs topographic mapping without affecting time of axon outgrowth, and that time of axon outgrowth directs topographic mapping without affecting *hox5* expression. The vagus motor neuron topographic map is therefore determined by two mechanisms that are acting in parallel: a *hox5*-dependent spatial mechanism akin to classic mechanisms of topographic map formation, and a novel axon outgrowth-dependent temporal mechanism in which time of axon formation is differentially regulated to direct axon targeting.

Table of Contents

Acknowledgments ..... **iii**

List of Figures and Tables ..... **vii**

Chapter 1: Introduction **1**
Mechanisms of topographic map development 2
Temporal influences on axon guidance 5
Vagus motor neuron development 6

Chapter 2: Materials and Methods **10**
Zebrafish care and maintenance 10
Generation of *hox* alleles and genotyping 10
hoxa5a morpholino 11
Plasmid construction and injection 12
Motor neuron transplants 13
Live imaging 14
RNA *in situ* hybridization 14
EdU labeling 14
Laser ablation 15
Cell picking, RNA isolation, and sequencing 15
Quantification and Statistical Analysis 17

Chapter 3: *hox5* genes instruct development of the vagus motor neuron topographic map **18**
Characterization of embryonic vagus motor neuron topographic map 18
Vagus motor neuron position determines axon target 20
hox5 expression distinguishes anterior and posterior mX neurons 21
Vagus motor neuron position determines *hox5* expression 22
Hox5 expression drives posterior axon targeting 23
Summary: *hox5* directs topographic mapping of posterior mX neurons 27

Chapter 4: Time of axon outgrowth instructs vagus topographic map development independently of *hox5* expression **42**
Axon formation and arrival in the periphery is delayed in posterior mX neurons 42
Vagus motor neuron position determines time of axon formation 43
Time of axon arrival in the periphery determines axon targeting 45
Hox5 expression and time of axon initiation direct mX axon targeting independently 47
Summary: Delayed axon initiation and outgrowth in posterior mX neurons directs posterior axon targeting 48

Chapter 5: Transcriptome analysis of anterior and posterior mX neurons **56**
Single cell picking allows RNA isolation from anterior versus posterior mX neurons 56
RNA-Seq dataset shows differential expression of *hox5* genes 57
Identification of genes that are enriched in anterior mX neurons 59
Identification of genes that are enriched in posterior mX neurons 63

Summary: Differential gene expression in anterior versus posterior mX neurons 65

Chapter 6: Conclusions and Future Directions 71

Hox5 expression drives posterior axon targeting 71

Time of axon initiation is regulated independently of birth order 74

Late axon arrival in the periphery drives posterior axon targeting 78

Temporal and spatial mechanisms act in parallel to direct topographic map development 80

References 83

Acknowledgments

First, I would like to thank my mentor Cecilia for her consistent and valuable support. It seems to be a rare thing to find a mentor who can train you both at and away from the bench, and I feel lucky to have had that experience. Thank you for teaching me how to read, write, and think like a scientist. Thank you for imbuing me with your scientific rigor and healthy skepticism of morpholinos. Thank you for sitting next to me in the dark for hours while we did our transplants; it was always such a pleasure working and chatting with you and I will remember it fondly.

I would also like to thank the members of the Moens Lab who have contributed to my training, especially my mentors Adam Miller and Minna Roh-Johnson. Adam, thank you for always challenging me and always inspiring me. Thank you for reminding me to see the big picture while never forgetting the details. Also thank you for that one time you stayed up past midnight to teach me how to backfill MLF neurons; it may have been the sleepless delirium, but I had a lot of fun that night. Minna, thank you for your example of strong and cheerful female leadership. Thank you for encouraging me to be direct and ambitious and strive towards what I want. I'm grateful for your guidance and your friendship. Additionally, I'd like to thank Chelsea Kidwell and Athea Vichas for their friendship and guidance during my time in the Moens Lab. Chelsea, thank you for your humor, encouragement, delicious baked goods, and wonderfully fun game nights at Grandma Charlotte's beach house. You are a dear and thoughtful friend. Athea, thank you for both raging at crazy political news with me and laughing at dumb Twitter jokes with me. Thank you for your strong, if ruthless, editing skills. I am a better scientist and

a better person because of my friendship with you. Finally, I acknowledge and thank the Moens Lab members whose technical support contributed to this work: to Arish Shah for his technical training and RNA wizardry, to Rachel Garcia for her excellent fish care and tireless and cheerful help with genotyping, to Jason Stonick for cloning the *hox5* constructs, and to Adam Isabella for help with mX neuron dissociation.

I would like to thank the members of my faculty committee for their guidance during my graduate career, and I am especially grateful to Boba Beronja and Dave Beier for their thorough reading of this dissertation. David Kimelman, thank you for being the first person to teach me how to work with zebrafish embryos; Dave Raible, thank you for your humor and cheer and for making sure I understand statistics; Boba Beronja, thank you for your kindness and encouragement—I've always left our meetings with invigorated confidence; and Dave Beier, thank you for your scientific and career guidance. I'd also like to thank the entire Beier family for your friendship and ski adventures over the years. Thank you Dave and Leah for always being willing to let us dog- and cat-sit, and thank you Molly, Cisco, and Snickers for the snuggles and comedic relief you provided when I was writing this dissertation at your house.

Thank you to those whose administrative support I relied on throughout graduate school. The Hutch has been a fantastic place to be a graduate student, and I would especially like to thank Karen Brighton, Pat Heath, Luna Yu, Maia Low, Marci Burden, and Marcie Buckner. Thank you also to the MSTP Directors Marshall Horwitz, Mary-Claire King, Julie Overbaugh, and Stephen Tapscott.

I would like to thank the women of the Seattle Ladies Choir for their friendship and for providing a dedicated 2 hours per week for me to think about something other than vagus motor neurons. Thank you for teaching me about music and creativity and individuality and feminism.

Finally, I thank my friends and family. To my Seattle framily: David, Lesley, Brad, Sheida, Eric, Jessica, Jaysen, Darwin—I am so grateful for all of you. Thank you for Bachelor viewing parties, excellent cheese plates, barbecues, game nights, Cruise Crew 2017, and always being willing to grab a beer with me. Thank you for your love, kindness, generosity, and humor. Thank you for adopting me and Matt as your own. I am so lucky to have friends like you.

To my Sea Ranch family: I deeply appreciate your love and support. Thank you for Bananagrams, hot tubs, beach walks, and the best damn New Year's Eve parties this world has ever seen. Thank you for raising me. I am honored to be one of yours. In particular, I would like to acknowledge the brilliant scientist Dr. David Cox. I am grateful for his influence on my life. One of the last conversations I remember having with Dave was about Francis Collins and DNA and the meaning of science and life while we walked next to the ocean. I'll never remember exactly what we said but I also know I'll never forget that conversation. I think of you often, Dave, and I love you.

To my brother and sister, Sam and Ellie—I could write another 100 pages about how much I love both of you and how proud I am of you. Being your sister is one of the great joys of my life. Thank you for your friendship and your humor and being wonderful

travel buddies. Thank you for loving me and supporting me, but also for challenging me and bringing me back down to earth when necessary. Thanks for listening to my intro to that one talk that one time, and for the excellent suggestions you made to improve it.

To my parents: Thank you for your inspiring examples and for raising me to ask lots of questions and think deeply. Mom, thank you for always telling me to stop worrying and take off my sweatshirt. Thank you for teaching me to always strive to be better. Dad, my favorite middle-aged science nerd: thank you for teaching me to look at and explore and ask questions about the natural world. Thanks for teaching me that MSTPs are a thing. I love talking science with you on long road trips. I hope we get to do that a lot more in the future. I love you both so much, and I am so deeply grateful for your support.

And finally, to my partner, Matt. I don't want to say that I couldn't have done this without you, because, you know, feminism. But I will say that it would have been a lot harder and a lot less fun. Thank you for all of the things. I love you chima.

List of Figures and Tables

Figure 1. Topographic mapping by larval vagus motor neurons. 28

Figure 2. Anterograde topographic mapping by larval vagus motor neurons. 30

Figure 3. Vagus motor neuron position determines axon target. 32

Figure 4. Expression of *hox* genes in rhombomere 8. 34

Figure 5. *hox5* expression distinguishes anterior and posterior mX neurons. 35

Figure 6. *hox5* genes are not required for vagus motor neuron topographic mapping.....37

Figure 7. *hox5* expression directs mX axons to posterior targets. 40

Figure 8. Time of axon formation and arrival in the head periphery is delayed in posterior mX neurons independently of birthdate. 49

Figure 9. Time of mX axon outgrowth determines peripheral target independently of hox5 expression. 51

Figure 10. Ablation of anterior mX neurons does not affect posterior mX axon targeting. 53

Figure 11. *hox5* acts independently of time of axon formation 54

Figure 12. Cell picking for RNA isolation. 66

Table 1. Individual tubes for RNA isolation. 68

Table 2. Samples used for RNA isolation and sequencing. 69

Table 3. List of selected genes that are differentially expressed between anterior and posterior mX neurons. 70

Chapter 1: Introduction

Neural maps are a common organizational motif in neurobiology and are crucial for the ability of animals to accurately perceive and respond to their external environment (Jason W. Triplett, 2014). In a neural map, neurons are systematically wired such that the position of the axon target reflects some underlying feature of the neuron. In some cases, referred to as discrete neural maps, axons project to a particular target based on the input parameter of that neuron (Luo & Flanagan, 2007). This is well exemplified by the olfactory map, where olfactory sensory neurons that express the same odorant receptor will project axons to the same discrete glomerulus in the brain (Imai, Sakano, & Vosshall, 2010). In other cases, referred to as continuous or, more commonly, topographic maps, the position of the axon target reflects the position of the cell body in space, preserving the neighbor-neighbor relationship between cell bodies and axon targets and creating representations of the outside world inside the brain (Cang & Feldheim, 2013; Luo & Flanagan, 2007). This often conjures images of sensory or motor homunculi, where outsized representations of body features are represented in the brain. In fact, these homunculi represent a circuit comprising multiple orders of neurons, rather than a single cell body projecting a single axon, and may be better thought of as specific behaviors rather than specific structures (Levine, Lewallen, & Pfaff, 2012; Rathelot & Strick, 2006). However, they illustrate the point effectively: the position of the neuron in the cortex reflects the position of the body feature that the neuron either senses or moves.

Precise coordination of cell body position and axon targeting is important for the development of neural circuitry. In spinal motor neurons, disruption of motor neuron positioning leads to disruptions of synaptic input specificity (Demireva, Shapiro, Jessell, & Zampieri, 2011). This can have functional consequences: loss of the transcription factor *Sat2b* in mice leads to altered positioning and wiring deficits of premotor interneurons, and these mice exhibit abnormal hindlimb hyperflexion in response to noxious stimuli (Hilde et al., 2016). Another example is seen in the tonoptopic map of sound frequency, where loss of the transcription factor *hox2* in mice leads to a failure of sound frequency discrimination (Karmakar et al., 2017). The arrangement of neurons into maps is also important for integration of sensory and motor systems (Cang & Feldheim, 2013). We are interested in understanding the development of topographic maps given their functional importance and prevalence throughout the nervous system.

Mechanisms of topographic map development

Previous investigations of topographic map development have described a spatial mechanism, where precise patterns of gene expression in neurons and their target areas direct axons to the proper location in a point-to-point matching system (Sperry, 1963; Jason W. Triplett & Feldheim, 2012). This mechanism has been particularly well-studied in the retinotopic map, where retinal ganglion cells (RGCs) in the nasal region of the retina project to the posterior superior colliculus (SC), and RGCs in the temporal region of the retina project to the anterior SC. A number of studies have demonstrated that this wiring pattern is mirrored by expression gradients of EphA receptors in the RGCs (high temporal-low nasal) and ephrinA ligands in the SC (high

posterior-low anterior) (Cheng, Nakamoto, Bergemann, & Flanagan, 1995; Connor, Menzel, & Pasquale, 1998; Drescher et al., 1995; Marcus, Gale, Morrison, Mason, & Yancopoulos, 1996). EphA+ RGCs are repelled by ephrinAs in culture, and ectopic expression of ephrinA2 in chick *in vivo* repels temporal but not nasal RGC axons (Drescher et al., 1995; Frisen et al., 1998; Nakamoto et al., 1996). Additionally, loss of ephrinA function *in vivo* leads to promiscuous targeting and topographic wiring deficits by temporal RGCs (Feldheim et al., 2000; Frisen et al., 1998; Pfeiffenberger, Yamada, & Feldheim, 2006). Interestingly, the RGCs are also patterned across the dorsal/ventral axis, such that dorsal RGCs project to the lateral SC and ventral RGCs project to the medial SC, and EphBs and ephrinBs have been implicated in topographic mapping along this axis (Hindges, McLaughlin, Genoud, Henkemeyer, & O'Leary, 2002; Mann, Ray, Harris, & Holt, 2002).

Similarly, in the limb-innervating motor neurons of the spinal cord, neurons are arranged into a map where dorsal limb-innervating neurons are located laterally in the spinal cord, and ventral limb-innervating neurons are located medially. The ventral versus dorsal limb-innervating neurons can be distinguished by mutually exclusive expression of the transcription factors Isl1 (ventral) and Lim1 (dorsal) (Landmesser, 1978; Tsuchida et al., 1994). Lim1 induces expression of EphA4, which mediates repulsive interactions from ephrinA4-expressing ventral limb mesenchyme (Kania & Jessell, 2003). Lim1+ neurons also express Ret, which mediates attraction to GDNF expressed in the dorsal limb (Kramer et al., 2006). Conversely, Isl1+ neurons express EphB1 and Unc5c, and are repelled from ephrinBs and Netrin-1 expressed in dorsal

limb mesenchyme, respectively (Luria, Krawchuk, Jessell, Laufer, & Kania, 2008; Poliak et al., 2015).

Spinal motor neuron topographic maps can be further refined into motor pools, which are groups of neurons innervating individual muscles of the limb. Different motor pools are defined by combinatorial expression of *Hox* family transcription factors. For example, in the chick, motor neurons innervating the flexi carpi ulnaris muscle express *Hoxa4* and *Hoxc4*, while motor neurons innervating the pectoralis muscle express *Hoxa4*, *Hoxc4*, and *Hoxc6*. Electroporation of *Hoxc6* RNAi to spinal motor neurons leads to a failure of pectoralis muscle innervation but has no effect on innervation of the flexi carpi ulnaris muscle (Dasen, Tice, Brenner-Morton, & Jessell, 2005). *Hox* genes also play an important role in topographic map formation in facial somatosensory neurons. Trigeminal neurons innervating different whiskers on the upper jaw of a mouse topographically project to rhombomere (r) 3 of the hindbrain and synapse onto second order neurons, which then project topographically to the thalamus, maintaining the grid-like representation of the whiskers (Erzurumlu, Murakami, & Rijli, 2010). *Hoxa2* is expressed in r3, and deletion of *Hoxa2* from r3 leads to an absence of topographic projections in both the hindbrain and thalamus (Oury et al., 2006). Amazingly, ectopic expression of *Hoxa2* in r2 is sufficient to create an ectopic somatosensory map in r2 of the hindbrain (Bechara et al., 2015). *Hoxa2* may direct somatosensory map formation through expression of Eph receptors in the hindbrain, reminiscent of the retinotopic map, as the absence of *Hoxa2* expression in r3 leads to a loss of EphA4 and EphA7 expression in r3 (Oury et al., 2006). Spatial patterning of gene expression is clearly

essential for topographic map formation; however, it is still unclear how a single *Hox* gene leads to the formation of intricate maps within a ubiquitous expression domain.

Temporal influences on axon guidance

In addition to classic spatial patterning, several studies have proposed that temporal patterning may be important for topographic map development. Studies of the Drosophila photoreceptor map have shown that the R7 and R8 photoreceptors, which target different layers of the medulla, are born at different times, leading to differential timing of axon outgrowth into the medulla (Kulkarni, Ertekin, Lee, & Hummel, 2016; Petrovic & Hummel, 2008). The transcription factor *sequoia* is sequentially expressed first in R8 and then in R7 during photoreceptor neurogenesis, and prolonged expression of *sequoia* in R7 and R8 or in R8 alone in an R7-deficient background directs all axons to the R7-innervating layer (Petrovic & Hummel, 2008). Additionally, studies of the mouse olfactory topographic map have shown that cell position correlates with birth order and therefore with time of axon arrival in the target region (Eerdunfu, Ihara, Ligao, Ikegaya, & Takeuchi, 2017). Axons from early-born Sema3F-expressing olfactory sensory neurons arrive in the dorsal olfactory bulb and deposit Sema3F protein to repel axons from later-born Neuropilin2-expressing olfactory sensory neurons, which are then restricted to the ventral bulb, indicating that time of neuron birth may direct topographic map development (Takeuchi et al., 2010). However, though these studies demonstrate correlation between temporal patterning and topographic connectivity, timing-based mechanisms for topographic map formation have been difficult to explicitly investigate, as they require live-imaging and the ability to manipulate the temporal environment. For

example, in the *Drosophila* photoreceptors, while prolonged *sequoia* expression alters axon targeting, it is not clear if this occurs via alterations in the time of axon growth into the medulla. In the mouse olfactory map, one would predict that delayed arrival of Sema3F-expressing neurons or early arrival of Neuropilin2-expressing olfactory neurons would lead to disruption in the map, but this prediction has not been tested. Furthermore, time of axon arrival in the target region typically correlates with neuron birth date, making it difficult to distinguish between the contribution of neuron identity due to birth order, and the contribution of axon arrival time. Here, we use the zebrafish embryo, with its rapid pace of nervous system development, accessibility to genetic and embryo manipulations, and amenability to live imaging to dissect the mechanisms of topographic map development.

Vagus motor neuron development

We use as our model for topographic map development the vagus motor neurons (also called motor neurons of cranial nerve X, or mX neurons). mX neurons are conserved throughout vertebrates, from lampreys to tetrapods, and are located in the caudal hindbrain (Gilland & Baker, 2005; Parker, Bronner, & Krumlauf, 2016). The anterior-posterior axis of the hindbrain neuroepithelium is patterned into segments, termed rhombomeres, that are defined by morphological boundaries and determined by patterns of *hox* genes expression (Krumlauf, 2016). The caudal hindbrain, often referred to as rhombomere 8 (r8), is recognized as distinct from the anterior hindbrain in that it is much larger that anterior hindbrain rhombomeres and it is not overtly segmented (Moens & Prince, 2002). Some studies, using a combination of fate maps and gene

expression studies in chick and mouse, have proposed that the territory classically referred to as r8 in fact contains up to 5 “cryptorhombomeres” (Cambronero & Puelles, 2000; Tomás-Roca, Corral-San-Miguel, Aroca, Puelles, & Marín, 2016). Consistent with this cryptic organization, in amniotes the mX neurons occupy two anatomically distinct nuclei in the caudal hindbrain, termed the nucleus ambiguus and dorsal motor nucleus of the vagus (Blumenfeld, 2010; Gilland & Baker, 2005). In fish, however, the mX neurons form a single apparently homogenous nucleus in r8 (Chandrasekhar, 2004; Gilland & Baker, 2005; Morita & Finger, 1985).

In humans, mX neurons located in the nucleus ambiguus innervate muscles derived from pharyngeal arches (PAs) 4 and 6, which include all striated muscles of the larynx and pharynx with the exception of the stylopharyngeus (innervated by CN IX) and tensor veli palatini (innervated by CN V) (Blumenfeld, 2010). mX neurons are therefore important for both speech and swallowing in humans (Matsuo & Palmer, 2008). We do not know of any congenital disorders affecting CN X in isolation, but pediatric dysphagia (difficulty swallowing) often involves CN X pathology and can have serious consequences including poor weight gain and increased risk for lung aspiration and infection (LaMantia et al., 2016). Children with 22q11 deletion syndrome, the most common microdeletion syndrome in humans, often experience dysphagia, and in mouse models CN X is often fused with CN IX (Karpinski et al., 2014). In adults, trauma, neurodegenerative disease, or vascular disease affecting mX neurons can present with dysphagia or dysarthria (difficulty speaking) (Erman, Kejner, Hogikyan, & Feldman, 2009). mX neurons in the dorsal motor nucleus of the vagus supply preganglionic

parasympathetic innervation to the thoracic and abdominal viscera, so CN X pathology can additionally present with dyspnea (difficulty breathing) (Erman et al., 2009). In zebrafish, mX neurons innervate muscles derived from PAs 4, 5, 6, and 7 (PA 5 and 7 were lost from mammalian lineages), so mX neurons control movement of the gill arches and the pharyngeal teeth (Higashijima, Hotta, & Okamoto, 2000; Schilling & Kimmel, 1997). Similar to mammals, zebrafish have a visceral branch of the vagus that innervates the gut (Olsson, Holmberg, & Holmgren, 2008).

Previous studies in both fish and mammals have used retrograde tracers injected into branches of the vagus nerve to show that the mX neurons in the adult animal are arranged topographically (Bieger & Hopkins, 1987; Morita & Finger, 1985). In mammals, for example, neurons in the anterior portion of the nucleus ambiguus innervate PA4 via the superior laryngeal branch, while neurons in the posterior nucleus ambiguus innervate PA6 via the recurrent laryngeal branch (Bieger & Hopkins, 1987). In fish, the mX neurons are similarly organized such that PA4-innervating neurons are at the anterior end of the vagal lobe, and PA7-innervating neurons are at the posterior end, though there is some overlap between neurons innervating neighboring PAs. In the fish oropharynx, the vagal gustatory system is similarly topographically organized, thought to be important for an oropharyngeal “food sorting” system where the fish can taste an object to determine whether it is food or detritus, and either ingest or expel the object accordingly (Morita & Finger, 1985). However, the mechanisms regulating development of the mX neuron topographic map remain unknown.

We describe two parallel and independent mechanisms for vagus topographic map development. First, we identify transcription factors that are specifically expressed in a subset of mX neurons. Members of the *Hox5* gene family are expressed in posterior mX neurons and posterior mX axon targets, and direct targeting of mX neurons towards posterior targets. In a second mechanism, we demonstrate that temporal regulation of axon formation influences axon targeting. While anterior and posterior mX neurons have similar birthdates, axons emerge from posterior mX neurons later than from anterior mX neurons, and late axon arrival in the peripheral target area directs axons to posterior targets. Finally, we demonstrate that these two mechanisms—the Hox5-dependent spatial mechanism and the axon growth-dependent temporal mechanism—are independent. This work therefore establishes a new mechanism of axon guidance, where time of axon formation can be regulated to direct axons to particular targets, that acts in parallel with *hox*-dependent spatial patterning mechanisms to govern the robust development complex topographic maps.

Chapter 2: Materials and Methods

Zebrafish care and maintenance

Danio rerio animals were raised at the Fred Hutchinson Cancer Research Center facility in accordance with IACUC-approved protocols. All experiments were carried out in accordance with IACUC standards. Fish were bred and maintained according to standard protocols (Kimmel, Ballard, Kimmel, Ullmann, & Schilling, 1995). For all embryo manipulations done between 23-35 hours post fertilization (hpf), embryos were staged according to the highly accurate prim staging method (Kimmel et al., 1995). Sex is not a relevant biological variable in our experiments, as they are carried out before sex is determined in zebrafish. Transgenic lines used in this study include *Tg(isl1-hsp70l:kaede)* (unpublished, Anita Ng and Victoria Prince) gift of the Prince Lab, *Tg(isl1:Gal4)fh452* (Davey, Mathewson, & Moens, 2016), *Tg(UAS:kaede)s1999* (Davison et al., 2007), gift of the Baier Lab, *Tg(isl1:mRFPfh1)* (Grant & Moens, 2010), *TgBAC(tcf21:mCherry-NTR)pd108* (J. Wang, Cao, Dickson, & Poss, 2015) and *Tg(isl1:GFP)rw0* (Higashijima et al., 2000). Transgenic lines generated for this study include *hoxb5a*^{GFP}*fh468* and *Tg(isl1:eGFPCAAX)fh474* (see details below).

Generation of *hox* alleles and genotyping

hoxb5a^{GFP} was generated using a CRISPR/Cas9-mediated knock-in strategy (Kimura, Hisano, Kawahara, & Higashijima, 2014). The donor plasmid was Mbait-hsp70-GFP, gift of the Higashijima lab. The CRISPR gRNA sequence was GTTACAAATGATGACGAGAC. Due to the possibility that plasmid insertion may disrupt endogenous *hoxb5a* expression, the *hoxb5a*^{GFP} line was maintained in a heterozygous

state. The *hoxb5a*^{fh477} and *hoxb5b*^{fh478} mutant alleles were all generated using the CRISPR/Cas9 method (Shah, Davey, Whitebirch, Miller, & Moens, 2015). *hoxb5a*^{fh477} is a 2 bp insertion that leads to an early stop codon at amino acid 187 in the protein, before the homeobox domain (see Figure 6A). *hoxb5b*^{fh478} is a 4 bp deletion that leads to an early stop codon at amino acid 186, before the homeobox domain (see Figure 6A). The CRISPR gRNA sequences were:

hoxb5a: GGAAGGGGGCGAAGAGCCTT

hoxb5b: GGTGGTCTGTGCTCCTTCCT

Genotyping was done using CRISPR-STAT primers to PCR (CRISPR-STAT fragments followed by gene-specific fragment) followed by restriction digest.

hoxb5a: Forward primer 5' tgtaaaacgacggccagtCCTTGTTCCAACAGCGAAA

Reverse primer 5' gtgtcttCTGGCCTCGTCGATTTCTGTAA

Digestion with BanII (New England Biolabs) generates a 147 bp WT product and a 57 bp + 92 bp mutant product.

hoxb5b: Forward primer 5' tgtaaaacgacggccagtACACATTTTGCGGACACA

Reverse primer 5' gtgtcttTAGTCGAGGTCGCCACAGATTC

Digestion with HpyAV (New England Biolabs) generates a 55 bp + 82 bp WT product and a 137 bp mutant product.

***hoxa5a* morpholino**

A splice-blocking morpholino from Gene Tools was obtained to prevent *hoxa5a* mRNA expression. The morpholino sequence is predicted to block the exon1 intron 1 splice junction: 5' CCTCTACGTTTGCCGTTTACCATGA. 4 ng of morpholino was injected at

the 1-cell stage. This concentration was chosen by balancing morpholino toxicity with efficiency of *hoxa5a* knockdown as assayed by RT-PCR on 24 hpf embryos. RNA was isolated from 10 embryos per condition using the Ambion RNAqueous Total RNA Isolation Kit (ThermoFisher AM1912). cDNA was amplified using the KAPA SYBR FAST One Step qRT-PCR Kit (KK4670) using the following primers:

hoxa5a forward: 5' TATCTAGCACCGCTGGCTCT

hoxa5a reverse: 5' GTGTCTGGTAGCGCGTGTAG

This creates a 243 bp WT amplicon. Morpholino is predicted to skip the exon 1 intron 1 splice junction and lead to a larger transcript.

The *rpl13a* gene was amplified as a control using the following primers:

rpl13a forward: 5' TCTGGAGGACTGTAAGAGGTATGC

rpl13a reverse: 5' AGACGCACAATCTTGAGAGCAG

This creates a 148 bp amplicon.

Plasmid construction and injection

The following plasmids were generated for this study: *isl1-hsp70:EGFP-CAAX*, *10XUAS:hoxa5a-p2a-EGFP-CAAX*, *10XUAS:hoxb5a-p2a-EGFP-CAAX*, and *10XUAS:hoxb5b-p2a-EGFP-CAAX*. The 10XUAS plasmid and EGFP-CAAX sequence were obtained from the Tol2kit (Kwan et al., 2007). The *islet1* promoter consisted of the zCREST enhancer upstream of hsp70 (Davey et al., 2016). The *hox* gene sequences were amplified from 24hpf cDNA using the following primers:

hoxa5a:	forward	ATGAGCTCTTATTTCGTCAATTCAT
	reverse	AGGCCGGTATCCGCTTCCTG

hoxb5a:	forward	ATGAGCTCTTACTTTGTAAACTCG
	reverse	TGGTTGGAAAGCGCTACCTG
hoxb5b:	forward	ATGAGCTCTTATTTTCTAAACTCG
	reverse	ATTTTGAAACGCGCTCCCCG

A pDONR 221 vector containing *p2a-NLSeGFP* (gift of Jeremy Rabinowitz) was modified to remove the NLS and add a CAAX domain for membrane localization. *hox* genes were cloned upstream of *p2a-eGFPCAAX.* Final DNA constructs were assembled in the pBHR4R3 plasmid (gift of the Brockerhoff lab) using the Gateway system (Life Technologies). Embryos were injected at the one-cell stage with 50 pg of plasmid together with 90 pg of Tol2 transposase mRNA. To create the *Tg(isl1:eGFPCAAX)fh474* line, injected embryos were raised to adulthood and outcrossed to identify germline-transmitting founders.

Motor neuron transplants

To track donor-derived cells, donor embryos were injected at the one-cell stage with 1% cascade-blue dextran (10,000 mw, Life Technologies). Before transplantation, embryos were anesthetized with 0.4% ethyl 3-aminobenzoate methanesulfonate (ms-222) (Sigma), and embedded in 1.4% low-melting point agarose (Gibco). Embedded embryos were immersed in normal Ringer's + ms-222. A small wedge of agar was removed to expose the head. A 10 μm diameter transplant pipette was inserted through the 4th ventricle into the hindbrain. Motor neurons were visualized using *Tg(isl1:kaede)* or *Tg(isl1:mRFP)* on a Zeiss AxioSkop fixed-stage microscope fitted with a 40X long working distance water-immersion lens. Motor neurons were removed from either the

anterior or posterior end of the vagus territory using an oil-controlled syringe mounted on a hydraulic micromanipulator (Kemp, Carmany-Rampey, & Moens, 2009) and transplanted to the anterior or posterior end of the host vagus territory, visualized by *Tg(isl1:GFP)* or *Tg(isl1:mRFP)*. After transplantation, embryos were unmounted from the agar and allowed to recover in embryo media. For time lapse experiments, embryos were given at least 1 hour of recovery time. For axon targeting experiments, embryos were imaged at 3 days post fertilization (dpf).

Live imaging

All images were collected on a Zeiss LSM 700 confocal microscope. For Kaede photoconversion, a region of interest was defined using morphological boundaries, and protein was photoconverted using the 405 laser at 10% power.

RNA *in situ* hybridization

Anesthetized embryos were fixed in 4% paraformaldehyde with 1X PBS (phosphate-buffered saline) and 4% sucrose at 4˚C overnight. The RNA *in situ* hybridization protocol was followed from (C. Thisse & Thisse, 2008). Following staining brain tissue was dissected, cleared step-wise into 75% glycerol, mounted, and imaged on a Zeiss Axioplan2 microscope. Probes for all *hox* genes were previously published (Prince, Joly, Ekker, & Ho, 1998; Prince, Moens, Kimmel, & Ho, 1998).

EdU labeling

Embryos were incubated in 0.5 mM (2'S)-2'-deoxy-2'-fluoro-5-ethynyluridine (EdU, Sigma T511293) diluted in fish water. Embryos were anesthetized and fixed at 48 hpf in 4% paraformaldehyde with 1X PBS and 4% sucrose for 30 minutes at room

temperature. After fixation, embryos were permeabilized in PBS + 0.5% TritonX100 for 30 minutes at room temperature, and brain tissue was dissected. To visualize EdU labeling, brains were incubated in a solution containing 10μM Cy5-azide (Lumiprobe A2020), 2 mM copper(II) sulfate (Sigma 45167), and 20 mM sodium ascorbate (Sigma A7631) for 1 hour at room temperature. Following incubation, brains were washed in PBS + 0.5% TritonX100 and processed for immunofluorescence using standard blocking and antibody incubations. The antibody used was chicken anti-GFP (1:250, Abcam).

Laser ablation

mX neurons were visualized using *Tg(isl1:kaede)* on a Zeiss LSM 780 confocal microscope. Individual mX neurons were ablated using the 2-photon laser at 35% power. Successful ablation was confirmed by immediate loss of all Kaede fluorescence and visible necrosis of the 10 μm diameter area previously occupied by the mX neuron. All neurons anterior to somite 1 were ablated.

Cell picking, RNA isolation, and sequencing

Embryos expressing *Tg(isl1:Kaede)* were anesthetized with ms-222 and embedded in 1.4% low-melting point agarose. At 28 hpf, when anterior mX neurons have initiated axon formation but posterior mX neurons have not, photoconversion was used to selectively label either the anterior-most quarter of mX neurons or the posterior-most quarter of mX neurons. Embryos were unmounted and transferred to calcium-free Ringer's solution + ms-222 (Westerfield, 2000). Rhombomere 8 was dissected from each embryo, using as morphological boundaries the posterior border of the otic vesicle

and the posterior border of somite 3 to ensure complete collection of all rhombomere 8 tissue. Dissected rhombomere 8 tissue from four embryos was combined into a single 0.2 mL Eppendorf tube with 20 uL of 0.25% Trypsin-EDTA (Gibco) and manually triturated for 5 minutes. All plastics were coated with Heparin (100 USP units/mL, BD PosiFlush) to prevent cell sticking. The tube was spun in a tabletop centrifuge for 10 seconds and 15 uL of trypsin solution was removed. 50 uL of 4°C Dulbecco's PBS (Gibco) + 5% fetal bovine serum (Fisher) + 1% bovine serum albumin (Sigma) was added to stop the trypsin reaction and cells were gently resuspended. This single-cell suspension was plated onto a glass coverslip and covered with mineral oil to prevent evaporation during cell picking. Cells were visualized on a Zeiss AxioSkop fixed-stage microscope fitted with a 10X lens. Appropriate mX neurons were selected by expression of red (photoconverted) Kaede and picked using a 10 μm diameter transplant pipette that was coated with Sigmacote (Sigma) and mounted on a hydraulic micromanipulator. mX neurons were transferred into a 0.2 mL Eppendorf tube with 40 uL of lysis buffer from the RNA isolation kit (see below) and immediately frozen at -80°C to preserve RNA. For all mX neurons, time between rhombomere dissection and freezing in lysis buffer was less than 90 minutes.

RNA was isolated using the RNAqueous-Micro Total RNA Isolation Kit (ThermoFisher). Tubes of frozen lysis buffer were thawed and combined to create 3 replicates of 100 anterior mX neurons or 3 replicates of 100 posterior mX neurons. After isolation, RNA was eluted in 10 uL of water.

cDNA amplification, library preparing, sequencing, and alignment was done in collaboration with the Genomics Core at Fred Hutchinson Cancer Research Center. cDNA was amplified using the SMART-Seq v4 Ultra Low Input RNA Kit for Sequencing (Clontech). Libraries were prepared using the Nextera XT DNA library prep kit (Illumina) and quality control was performed after library preparation with TapeStation and Qubit. Sequencing was performed on Illumina HiSeq.

After sequencing, reads were selected for Illumina's base call quality threshold and aligned to genome assembly GRCz10 using TopHat v2.1.0 (http://ccb.jhu.edu/software/tophat/indx.shtml). Read counts for each gene were generated using htseq-count v0.6.1p1, using the intersection-strict overlapping mode (http://www-huber.embl.de/users/anders/HTSeq/doc/count.html). Genes that didn't have at least 1 count/million in at least 2 samples were removed. Data was normalized and significance testing was performed using the exact test method in edgeR v3.18.1 (http://www.bioconductor.org/packages/release/bioc/html/edgeR.html). Genes were called significantly differentially expressed if log(fold change) ≥ 0.585 and false discovery rate $\leq 5\%$.

Quantification and Statistical Analysis

Statistical analysis was done using GraphPad Prism for all tests except for transplant experiments that used 2x3 Fisher's exact test (Figure 2), which was done using Vassar Stats. Statistical details are noted in figure legends. For all figures, *, $p < 0.05$; **, $p < 0.01$; ***, $p < 0.001$; ****, $p < 0.0001$.

Chapter 3: *hox5* genes instruct development of the vagus motor neuron topographic map

Characterization of embryonic vagus motor neuron topographic map

To understand how the mX neuron topographic map is established, we first determined whether the mX neuron map is present in the zebrafish embryo. We used the *Tg(isl1:Kaede)* line which expresses the cytoplasmic photoconvertible protein Kaede in postmitotic branchiomotor neurons including mX neurons (Anita Ng and Victoria Prince, unpublished). mX neurons are born ventrally in hindbrain r8 and migrate dorsolaterally to form the vagus motor nucleus by 36 hours post fertilization (hpf) (Ohata et al., 2009). Axons emerge basally, first exit the hindbrain at 27 hpf, and travel anteriorly in a single fascicle before making a characteristic ventral turn at the otic vesicle towards the pharyngeal arches (PAs) (Figure 1A) (Cox, Lamora, Johnson, & Voigt, 2011). The axons divide peripherally into 5 separate branches, which are all present by 3 days post fertilization (dpf): 4 branches that innervate PA4, 5, 6, and 7, and a 5^{th} posterior branch that innervates visceral targets (Figure 1A) (Higashijima et al., 2000). In time lapse movies, axon branches appear sequentially in an anterior-to-posterior order, with the PA4 branch emerging first and the PA7 branch emerging last (Figure 1B, Movie S1). This corresponds with the sequential anterior-to-posterior development of the pharyngeal arches themselves (Schilling & Kimmel, 1997). The visceral branch appears at about the same time as PA5 (Figure 1B, Movie 1). To visualize the timing of mX axon outgrowth relative to PA development, we used the *Tg(isl1:eGFPCAAX)* line as a membrane marker for postmitotic motor neurons, and combined it with the

Tg(tcf21:mCherry) line, which marks head mesoderm in the core of the PAs and PA arteries (Nagelberg et al., 2015; J. Wang et al., 2015). As expected, mesodermal *tcf21*+ cells are seen in establishing PAs in sequential anterior-posterior order before mX axon innervation, with PA5 forming before axons are present in PA4, and PA6 forming before axons are present in PA5 (Figure 1C, Movie 2). mX axons extend into the *tcf21*+ mesodermal core of the PAs, which later develop into the head musculature (Nagelberg et al., 2015).

To visualize the mX neuron topographic map in the embryo, we used the *Tg(isl1:Kaede)* line to retrogradely label the motor neurons that innervate specific PAs. By photoconverting the PA4 branch, we found that neurons innervating PA4 are located at the anterior-most end of the mX territory (Figure 1D,G). Neurons innervating PA7 lie posterior to PA4-innervating neurons (Figure 1E,G), while neurons in the visceral branch are at the posterior-most end of the mX territory (Figure 1F,G).

In a complementary approach, we photoconverted mX cell bodies and anterogradely tracked axons to the PAs. We used the somites, which flank the mX territory, as morphological boundaries to divide the mX territory into 5 regions along the anterior-posterior axis of r8, and photoconverted neurons in each region. We found that neurons at the anterior end of the mX territory (regions 1 and 2) innervated PAs but not the viscera, while neurons at the posterior end (regions 4 and 5) primarily innervated the viscera and not the PAs (Figure 2B,C,E,F,G). Neurons in the middle of the mX territory (region 3) innervated both PAs and viscera, but never innervated the anterior-most target, PA4 (Figure 2D,G). Additionally, when we restricted photoconversion to 20 μm at

the most anterior end of the mX territory, we found those neurons almost exclusively innervated PA4 (Figure 2A,G). Taken together, our photoconversion experiments reveal that the position of the cell body along the anterior-posterior axis of r8 correlates with its target along the anterior-posterior axis of the pharyngeal arches. This zebrafish larval topographic map is not as well resolved as the adult vagus topographic map of goldfish, where neurons innervating PA4 and PA7 do not overlap (Morita & Finger, 1985). Nevertheless, it was sufficiently resolved for us to study its development.

Vagus motor neuron position determines axon target

We next sought to determine whether the position of an mX neuron in r8 determines its axon target. To address this question, we used single-neuron transplantation to manipulate the spatial environment of individual postmitotic neurons (Eisen, 1991). At 27 hpf, when postmitotic mX neurons are present along the anterior-posterior axis of r8 but before they have extended axons, we transplanted nascent mX neurons from a *Tg(isl1:Kaede)* donor to the same (homotopic) or different (heterotopic) positions in r8 of a *Tg(isl1:GFP)* host embryo. To ensure accurate developmental age, we used the highly precise “prim staging” method to stage all embryos at the time of transplantation (see Materials & Methods for details). We transplanted 1-5 mX neurons (median = 2) into each host embryo, allowed the host to develop to 3 dpf, and then assessed targeting of the donor neuron(s) (Figure 3A). In all cases where only one donor mX neuron was present, that neuron innervated only one mX axon branch (n = 8/8 embryos; e.g. Figure 3B,E). As expected, in control anterior → anterior homotopic transplants, donor neurons innervated primarily anterior targets (Figure 3B,F), and in

control posterior → posterior homotopic transplants, donor neurons innervated primarily posterior targets (Figure 3D,F). In heterotopic anterior → posterior transplants, donor neurons innervated primarily posterior targets (Figure 3C,F). Likewise, in heterotopic posterior → anterior transplants, donor neurons innervated primarily anterior targets (Figure 3E,F). These results show that the anterior-posterior position of an mX neuron in r8 determines its peripheral target.

hox5 expression distinguishes anterior and posterior mX neurons

In order to understand how cell position determines axon target, we set out to identify differences between anterior and posterior mX neurons. *Hox* genes are well known for their role in patterning the anterior-posterior axis of the vertebrate hindbrain including motor neurons; however, a role in vagus-specific topographic mapping has not been described (Philippidou & Dasen, 2013). We therefore sought to determine whether *hox* genes were differentially expressed in anterior versus posterior mX neurons by RNA *in situ* hybridization at 27 hpf. We focused on *hox4*, *hox5*, and *hox6* paralogs which are known to have anterior expression limits in the posterior hindbrain and anterior spinal cord (Bruce, Oates, Prince, & Ho, 2001; Hortopan & Baraban, 2011; Prince, Joly, et al., 1998; Prince, Moens, et al., 1998). We found that *hox4* genes have anterior borders anterior to the mX territory, and *hox6* genes have anterior borders posterior to the mX territory (Figure 4). However, *hoxa5a*, *hoxb5a*, and *hoxb5b* all have diffuse anterior borders of expression within the mX territory (Figures 4E-H, 5A). *hoxc5a* was not detectable in the hindbrain. Using morphological boundaries and double RNA *in situ* hybridization with *tbx20* to mark motor neurons, we demonstrated that *hoxa5a*,

hoxb5a, and *hoxb5b* are expressed in the posterior third (approximately 50 μm) of the mX territory (Figure 4E-H).

To visualize *hox5*-expression with high resolution in living animals, we used a CRISPR/Cas9 approach to target GFP to the endogenous *hoxb5a* locus (see Materials & Methods for details). Consistent with RNA *in situ* expression data at 27 hpf, *hoxb5a*^{GFP} is expressed in a graded pattern, with a combination of GFP+ and GFP- cells at the anterior end of the mX territory (corresponding to regions 1 and 2 from Figure 2), while 100% of cells in the posterior mX territory (regions 3, 4, and 5 from Figure 2) are GFP+ (Figure 5). The anterior limit of *hoxb5a*$^{GFP+}$ expression appears more anterior than the corresponding *hoxb5a* mRNA expression (Figure 5A compared to 5B). This difference likely reflects perdurance of the GFP protein from an earlier, broader domain of expression, as we also detected GFP expression throughout the spinal cord at 27 hpf although *in situ* hybridization in *hoxb5a*$^{GFP+}$ embryos confirmed that CNS expression of *hoxb5a* mRNA was more restricted at this stage (data not shown). *hoxb5a*^{GFP} is also expressed in PA6 and PA7 (Figure 5C). Thus, *hox5* genes are expressed in posterior mX neurons and their posterior PA targets, suggesting *hoxb5a* expression may direct posterior mX axon targeting.

Vagus motor neuron position determines *hox5* expression

Our RNA *in situ* hybridization and *hoxb5a*^{GFP} reporter demonstrated that mX neuron position correlates with *hox5* expression. We next asked whether mX neuron position *determines hox5* expression by transplanting postmitotic mX neurons at 27 hpf from donor embryos that carried the *hoxb5a*^{GFP} reporter into *hoxb5a*^{GFP}-negative host

embryos, and assessing GFP expression in donor mX neurons at 3 dpf. As expected, 100% of donor mX neurons (n = 13 neurons) maintained GFP expression in control homotopic posterior → posterior transplants (Figure 5F). Conversely, as expected in control anterior → anterior transplants, only 23% of donor mX neurons (n = 22 neurons) were GFP+ (Figure 5D,F). However, when anterior mX neurons were transplanted heterotopically into posterior r8, 64% (n = 28 neurons, p = 0.0046 by Fisher's exact test compared to anterior → anterior) of the donor mX neurons were GFP+ (Figure 5E,F). Due to GFP perdurance, we were not able to assess *hoxb5a* downregulation in posterior → anterior transplants. These results suggest that the position of an mX neuron in r8 determines its *hox5* expression. The ability of transplanted post-mitotic neurons to turn on expression of *hoxb5a* (Figure 5) and to change their axon targeting after transplantation (Figure 4) indicates that mX neuron fate remains plastic after birth.

***Hox5* expression drives posterior axon targeting**

Our transplant experiments demonstrated that mX neurons positioned in anterior r8 will be *hox5*-negative and will innervate anterior axon targets. Conversely, mX neurons positioned in posterior r8 will be *hox5*-positive and will innervate posterior axon targets. We therefore hypothesized that *hox5* expression may determine mX axon targeting.

To test the role of *hox5* genes in mX topographic mapping, we used the CRISPR-Cas9 system and designed guides to exon 1 of *hoxb5a* and *hoxb5b* with the goal of making a deleterious mutation in each gene. For *hoxb5a*, we recovered a 2 bp insertion that lead to an early stop codon at amino acid 187, before the homeobox

domain (*hoxb5a*^{fh477}, Figure 6A). For *hoxb5b*, we recovered a 4 bp deletion that lead to an early stop codon at amino acid 186, before the homeobox domain (*hoxb5b*^{fh478}, Figure 6A). For *hoxa5a*, we elected to knockdown *hoxa5a* function with a morpholino to improve speed and frequency of recovering a triple *hox* knockdown embryo. We titrated the *hoxa5a* to a 4 ng bolus at the single-cell stage, which minimized toxicity but maximized *hoxa5a* knockdown, as shown by RT-PCR on 24 hpf embryos (Figure 6A,B, see Materials & Methods for details).

We hypothesized that *hox5* function is required for accurate targeting of posterior mX neurons, as *hox5* genes are expressed in posterior mX neurons and their peripheral targets, and predicted that posterior mX axon branches may be absent in *hox5* mutants. However, we found that all mX axons branches were present in 100% of *hoxb5a*^{fh477} mutants, 100% of *hoxb5b*^{fh478} mutants, and 87.5% of *hoxa5a* morphants (Figure 6C-G, n = 6 embryos *hoxb5a*, n = 12 embryos *hoxb5b*, n = 8 embryos *hoxa5a* MO, p = ns for each condition by Fisher's exact test compared to WT sibs where n = 11 embryos). In 1/8 *hoxa5a* morphant embryos, the PA6 branch was absent, which may be due to morpholino toxicity, as there were also non-specific effects on cell migration (Figure 6D,G) as well as a variable level of necrosis in injected embryos (data not shown). Similarly, when we injected the *hoxa5a* morpholino into the *hoxb5a*^{fh477}*;hoxb5b*^{fh478} double mutants (which we will refer to as triple mutants), we found that all mX branches were present in 85% of embryos (n = 20 embryos, p = ns by Fisher's exact test compared to WT sibs). In 3/20 triple mutant embryos, the PA6 branch was absent,

which again may be due to morpholino toxicity. These results suggest that *hox5* genes are not required for posterior mX axon branches.

To determine whether *hox5* genes are required for the mX neuron topographic map, we sought to assay axon targeting based upon mX neuron position. We therefore used our Kaede photoconversion approach to assay targeting of posterior mX neurons in the *hox5* mutants. We used the same morphological boundaries as previous photoconversion experiments (see Figure 2) and photoconverted mX neurons in region 3 or region 4. For both regions, we saw no significant difference in posterior mX neuron targeting in *hoxa5a* morphants, *hoxb5a*^{fh477} mutants, *hoxb5b*^{fh478} mutants, or triple *hox5* mutants (Figure 6D-I). (For region 3, WT sibs n = 10 embryos, *hoxa5a* n = 4 embryos, *hoxb5a* n = 4 embryos, *hoxb5b* n = 8 embryos, triple mutants n = 9 embryos, p = ns comparing each condition to WT sibs. For region 4, WT sibs n = 10 embryos, *hoxa5a* n = 10 embryos, *hoxb5a* n = 7 embryos, *hoxb5b* n = 12 embryos, triple mutants n = 10 embryos, p = ns comparing each condition to WT sibs.) These results suggest that *hoxa5a*, *hoxb5a*, and *hoxb5b* are not required for proper targeting of posterior mX neurons.

We next turned to a targeted gain-of-function approach to determine whether *hox5* genes are sufficient to direct mX axon targeting. We constructed plasmids encoding *UAS:hox5gene-p2a-EGFPCAAX* and injected the DNA into 1-cell stage embryos expressing *Tg(isl1:Gal4);Tg(isl1:mRFP)*. This strategy allowed us to generate embryos with membrane-GFP-labeled *hox5*-expressing neurons scattered sparsely throughout the vagus territory (Figure 7A-D). There was no significant difference in

distribution of *hox5*-expressing mX neurons compared to mX neurons expressing a control *isl1:eGFPCAAX* construct (Figure 7E). If *hox5* directs axons towards posterior targets, we predicted that *hox5*-expressing mX neurons would innervate posterior targets with higher frequency than anterior targets. When mX neurons were labeled with a control *isl1:eGFPCAAX* construct, labeled neurons innervated all peripheral branches with equal frequency (Figure 7A,F). In contrast, *hoxa5a*-, *hoxb5a*-, or *hoxb5b*-expressing mX neurons exhibited a strong bias towards innervating posterior branches (Figure 7B-D).

To examine whether *hox5* expression truly disrupts the mX topographic map, we determined whether axons mistarget based upon the position of a *hox5*-overexpressing neuron. Because all mX axons fasciculate in a single peripheral nerve before branching into the PAs, we can't distinguish axons of individual expressing mX neurons. We therefore limited our analysis to embryos that had labeled neurons in the anterior-most 20 μm of the mX territory that normally innervate PA4 exclusively (the "PA4 zone," Figure 2A,G). We found that in embryos expressing the control construct, 89% of the embryos that had labeled cells in the PA4 zone also had labeled axons in the PA4 branch (Figure 7G), consistent with our photoconversion data. However, in embryos with *hox5*-expressing neurons in the PA4 zone, though *hox5*-expressing neurons are capable of innervating PAs (Figure 7F), only 41% (*hoxa5a*), 11% (*hoxb5a*), or 31% (*hoxb5b*) of the embryos had labeled axons in the PA4 branch (Figure 7G). Together, these results strongly suggest that *hox5* expression directs axon targeting to posterior targets.

Summary: *hox5* directs topographic mapping of posterior mX neurons

In this chapter, we have used a photoconversion approach to characterize for the first time the vagus motor neuron topographic map in the larval zebrafish, showing that cell position correlates with axon target position. Furthermore, our single-neuron transplant approach establishes that cell position *determines* axon target position. We demonstrate that *hox5* expression correlates with cell position, such that an mX neuron born in posterior r8 or transplanted into r8 will express *hox5* genes. Finally, we use an ectopic expression approach to demonstrate that *hox5* expression influences topographic map formation by directing posterior mX neuron targeting to posterior peripheral targets.

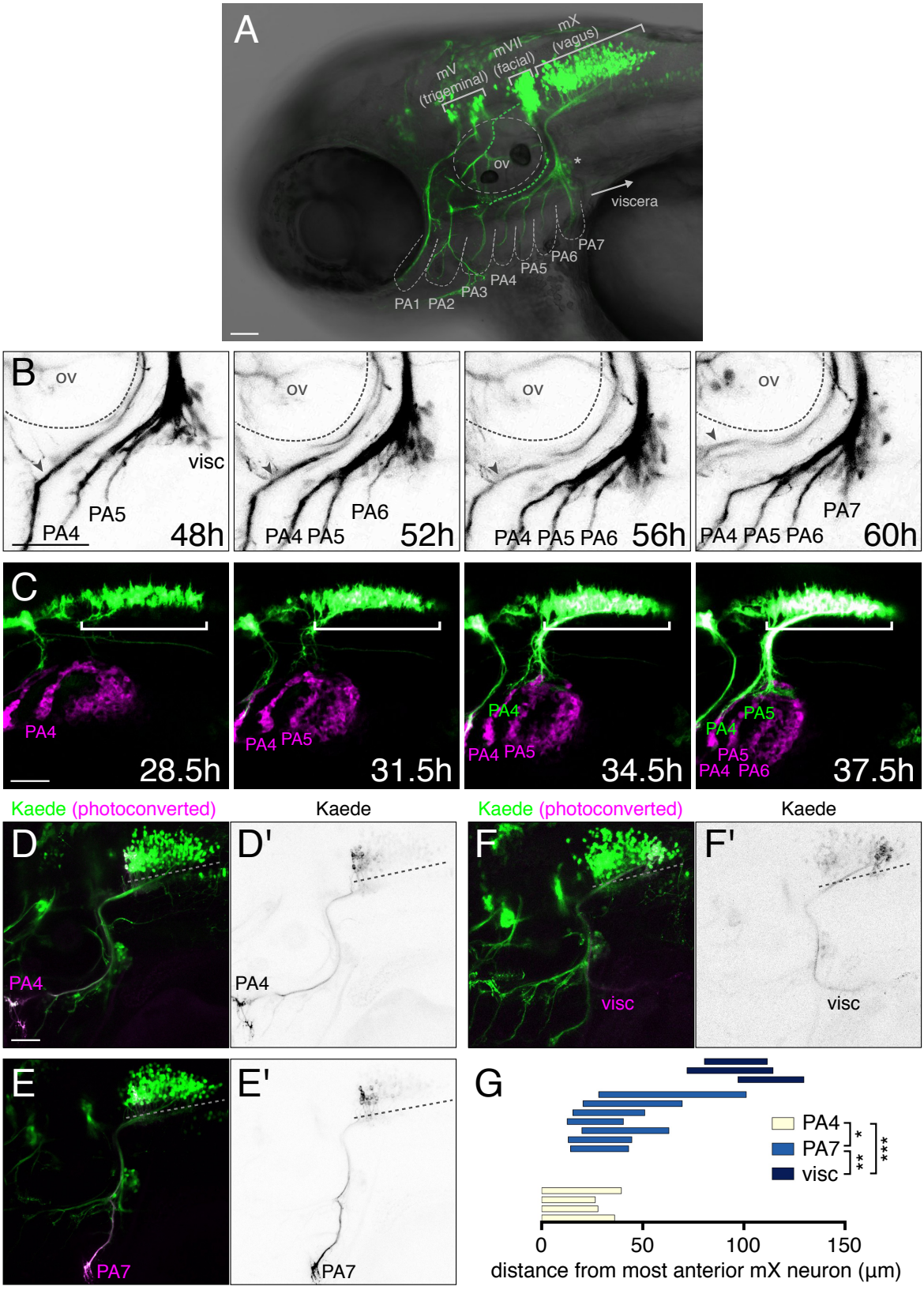

Figure 1. Topographic mapping by larval vagus motor neurons.

(A) Lateral view of a larval zebrafish expressing *Tg(isl1:Kaede)* at 3 dpf. Brackets mark the location of cranial motor nuclei, as named. Dotted line marks pharyngeal arches (PA), dotted circle marks the otic vesicle (ov), and asterisk marks a subset of vagus sensory cells that are labeled by *islet1*. (B) mX axon branches innervate PAs in sequential order from anterior to posterior in embryo expressing *Tg(isl1:Kaede)*. Gray arrowhead indicates cranial nerve IX. See also Movie 1. (C) Mesodermal *tcf21+* cells (magenta) organize into PAs sequentially from anterior to posterior. mX axons (green) then extend into *tcf21+* territory in sequential anterior-posterior order. White bracket indicates mX territory. See also Movie 2. (D-F) Photoconverted Kaede in a single one of the mX axon branches at 4 dpf is shown in magenta and (D'-F') black. Dotted lines mark the length of the mX territory. PA4-innervating neurons are at the anterior edge of the mX territory, PA7-innverating neurons are posterior to PA4 neurons, and viscera-innervating neurons are at the posterior-most end of the mX territory. Due to the small scale of the region, we were not able to photoconvert PA5 or PA6 alone. (G) Quantification of axon photoconversion experiments. Each bar represents a single embryo. Analysis done using unpaired t test comparing anterior and posterior borders of photoconverted population. Anterior is left and dorsal is up, and scale bars are 50 μm.

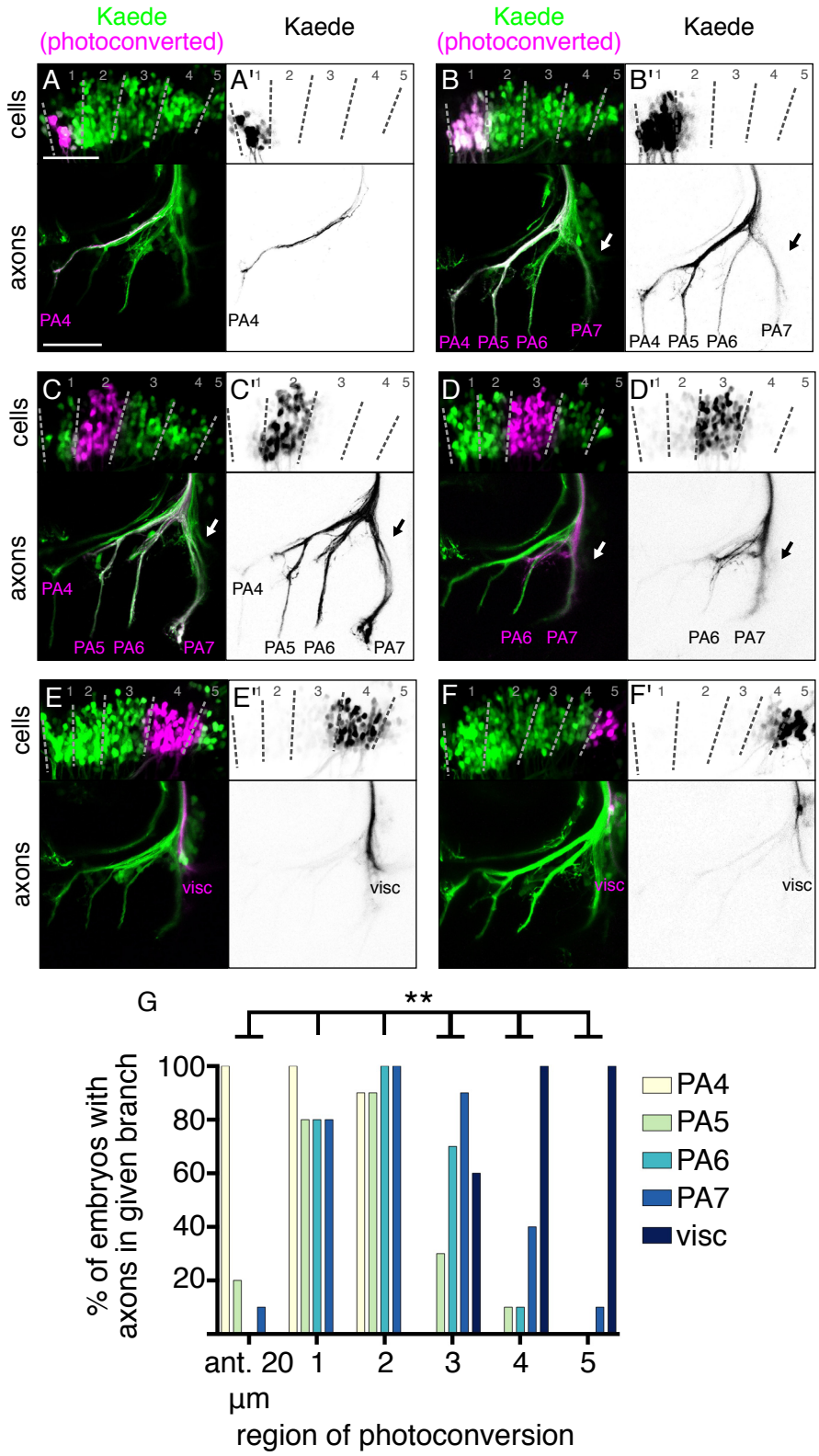

Figure 2. Anterograde topographic mapping by larval vagus motor neurons.

(A-F) Photoconverted Kaede in cell bodies is shown in magenta and (A'-F') black with anterior left and dorsal up. Bottom panels show photoconverted Kaede in peripheral axon branches. (A,A') The anterior-most 20 μm of the mX territory was photoconverted. (B-F,B'-F') 5 regions were defined using somite boundaries, with the anterior border of region 1 aligning with the anterior border of somite 1, and the posterior border of region 5 extending halfway into somite 2. Cells in a single region were photoconverted. (G) Quantification of (A-F). n = 10 embryos per region photoconverted. Analysis was done using Chi-square test comparing regions in pairwise combinations with respect to each axon branch. Regions are considered different if they differ in at least one branch. Anterior is left and dorsal is up, and scale bars are 50 μm.

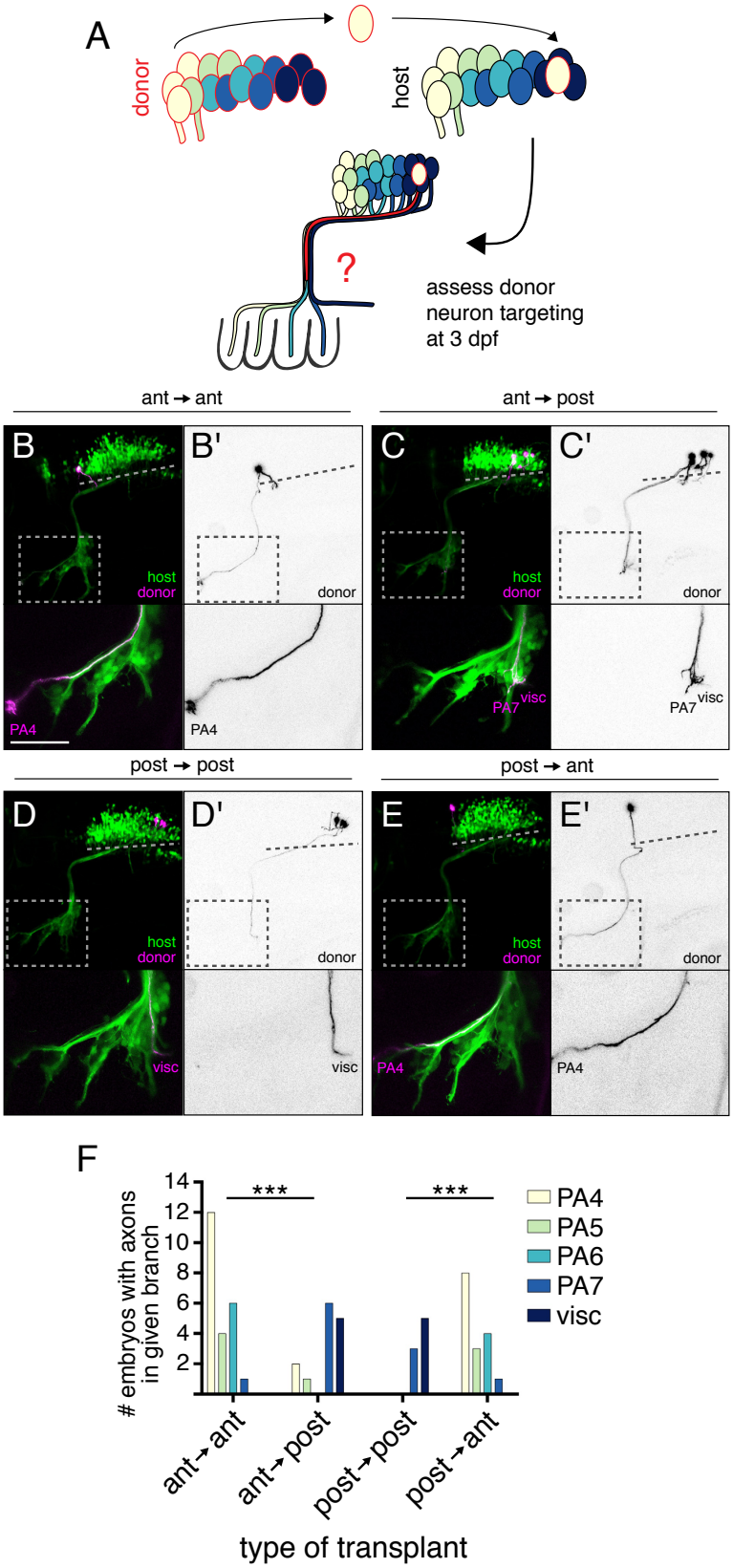

Figure 3. Vagus motor neuron position determines axon target.

(A) Schematic of postmitotic neuron transplantation approach. mX neurons are transplanted homotopically or heterotopically (pictured) before axon formation and donor axon targeting is assayed at 3 dpf. Colors represent mX neurons innervating different peripheral targets. (B-E) Anterior mX neurons transplanted homotopically (B) innervate anterior targets while anterior mX neurons transplanted heterotopically (C) innervate posterior targets. Posterior mX neurons transplanted homotopically (D) innervate posterior targets while posterior mX neurons transplanted heterotopically (E) innervate anterior targets. Donor neurons are marked by *Tg(isl1:kaede)* in magenta and black-on-white (B'-E'). Host motor neurons are marked by *Tg(isl1:GFP)* in green. Dotted lines indicate the length of the mX territory, dotted boxes indicate region shown in bottom panels. (F) Quantification of transplant results showing number of host embryos with a donor axon in a given branch. Statistical analysis done by using Fisher's exact test (see STAR Methods for details). Ant → ant n = 14 host embryos; ant → post n = 12; post → post n = 7; post → ant n = 12. Anterior is left and dorsal is up, and scale bars are 50 μm.

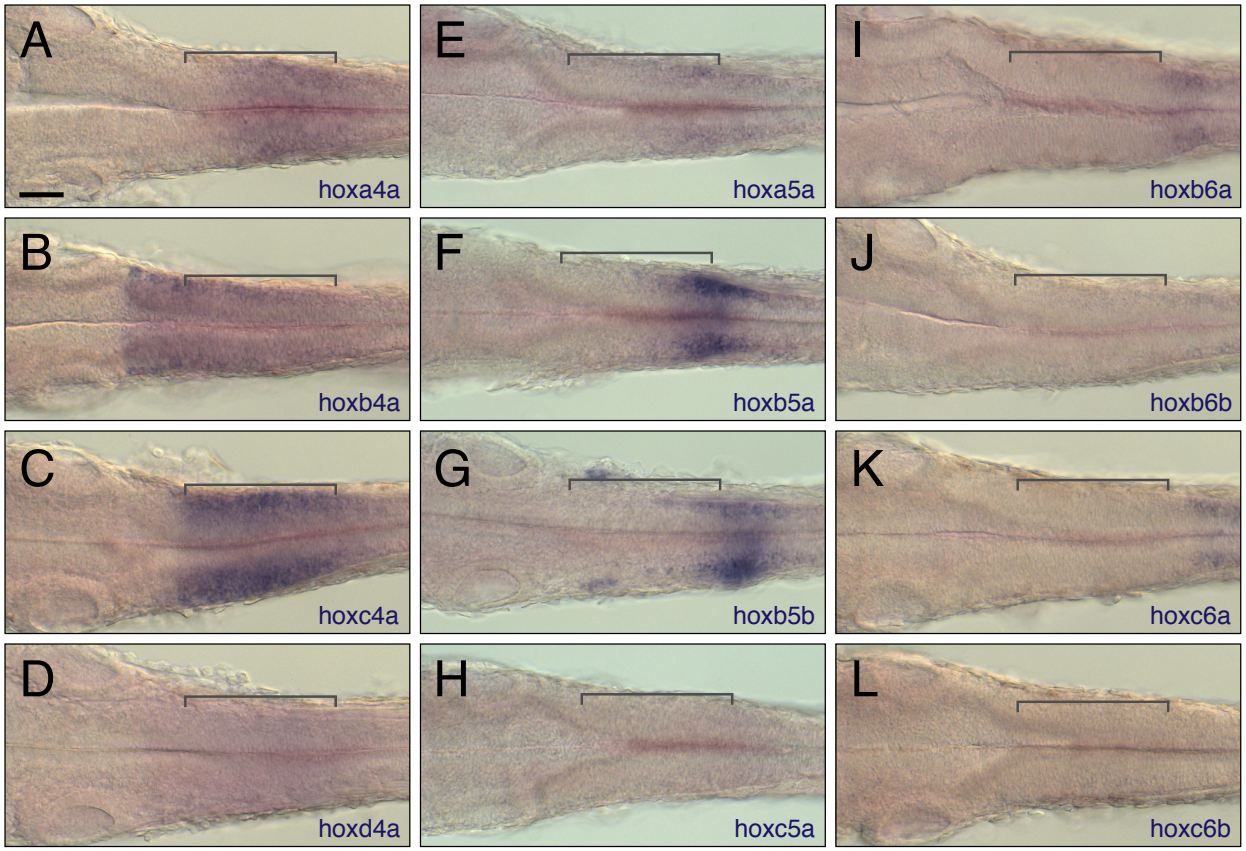

Figure 4. Expression of *hox* genes in rhombomere 8.

(A-L) RNA *in situ* hybridization at 27 hpf showing *hox* gene expression in purple. Brackets indicate mX territory. *hoxa5a*, *hoxb5a*, and *hoxb5b* are all expressed in posterior but not anterior r8. Dorsal view with anterior to the left, and scale bars are 50 μm.

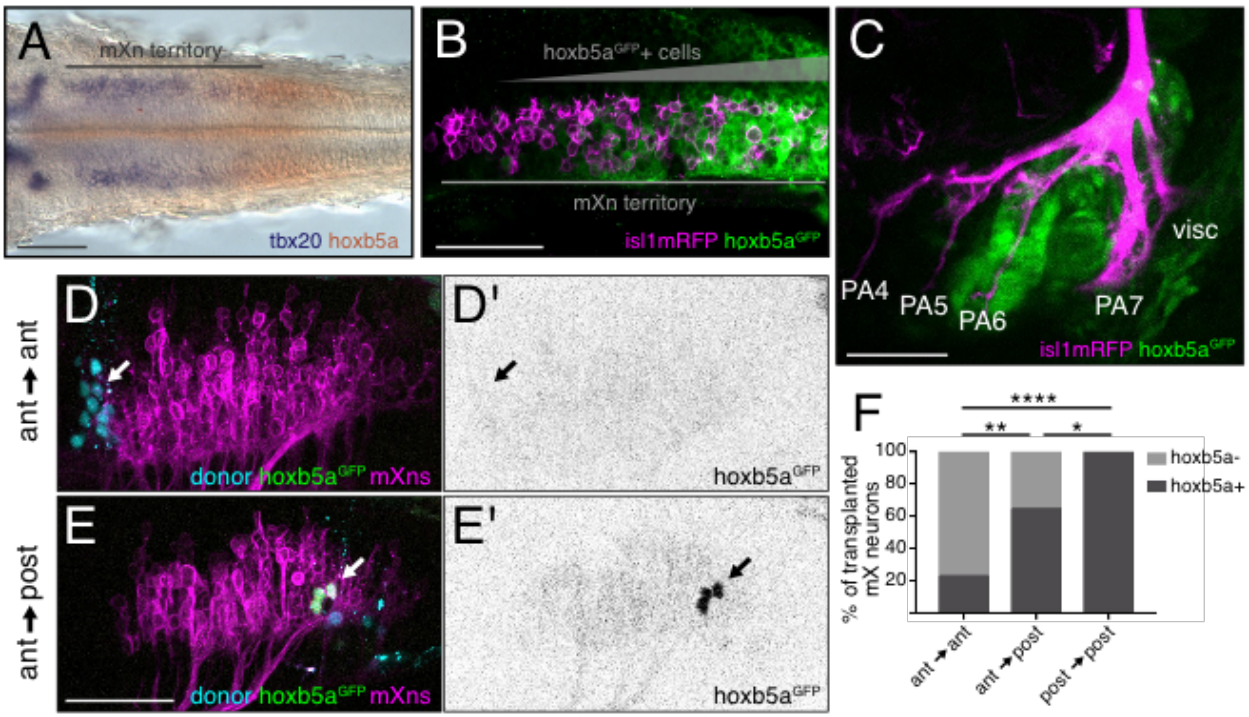

Figure 5. *hox5* expression distinguishes anterior and posterior mX neurons.

(A) *hoxb5a* is expressed in the posterior mX territory. RNA *in situ* hybridization at 27 hpf showing *hoxb5a* expression in red and *tbx20* expression, which marks postmitotic motor neurons, in purple. Dorsal view, anterior to left. (B,C) *hoxb5a*^{GFP} is expressed in posterior mX neurons, PA6, and PA7, but not in anterior mX neurons or anterior PAs. *hoxb5a*^{GFP} is shown green and *Tg(isl1:mRFP)* is shown in magenta at 27 hpf (B) or 3 dpf (C). (D,E) Anterior mX neurons transplanted homotopically are *hoxb5a*-negative (arrow in D), while anterior mX neurons transplanted heterotopically to posterior r8 are *hoxb5a*-positive (arrow in E). Donor embryos contain cascade blue vital dye (cyan) and express *Tg(isl1:mRFP)* (magenta) and *hoxb5a*^{GFP} (green and (D',E') black). Host embryos express only *Tg(isl1:mRFP)*. (F) Quantification of (D,E). Donor mX neurons are identified by coexpression of cascade blue and *Tg(isl1:mRFP)*. Shown is percentage of donor mX neurons expressing *hoxb5a*^{GFP}. Analysis done by Fisher's

exact test. Ant → ant n = 22 neurons, 6 embryos; ant → post n = 28 neurons, 9 embryos; post → post n = 13 neurons, 5 embryos. In (B-E), anterior is left and dorsal is up. In all images, scale bars are 50 μm.

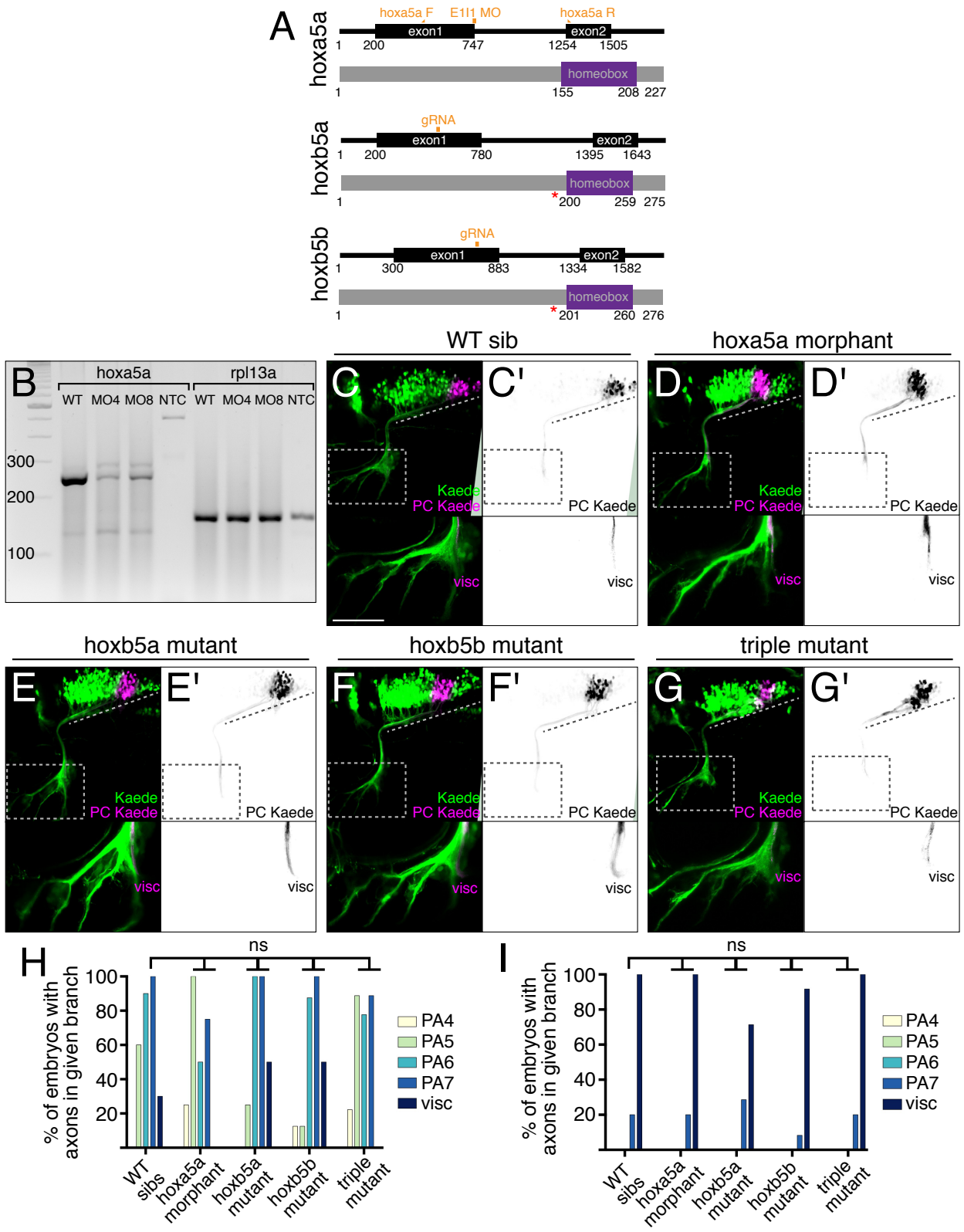

Figure 6. *hox5* genes are not required for vagus motor neuron topographic mapping.

(A) Schematic of *hox5* genes (black, top lines) and proteins (gray and purple, bottom lines). Top, *hoxa5a* morpholino targeting the exon1 intron1 splice junction and RT-PCR primers to assay knockdown are shown in orange. Middle, guide RNA targeting exon 1 of *hoxb5a* shown in orange. We recovered a frame shift allele, *fh477*, which led to an early stop codon before the homeobox domain (red asterisk). Bottom, guide RNA targeting exon 1 of *hoxb5a* shown in orange. We recovered a frame shift allele, *fh478*, which led to an early stop codon before the homeobox domain (red asterisk). (B) RT-PCR showing amplification of *hoxa5a* (using primers from (A)) or *rpl13a* as a control. WT, wild-type uninjected embryos, MO4, embryos injected with 4 ng *hoxa5a* morpholino, MO8, embryos injected with 8 ng *hoxa5a* morpholino, NTC, no template control. WT *hoxa5a* product is 243 bp, WT *rpl13a* amplicon is 148 bp. (C-G) Photoconverted Kaede in region 4 (defined by posterior half of somite 2, see Figure 2) shown in magenta and (C'-G') black in WT sibling (C) or *hox5* deficient embryo (D-G). In *hox5* deficient embryos, all mX axon branches are present and posterior mX neurons target posterior (visceral) branches appropriately. (H) Photoconversion experiments of mX neurons in region 3 (defined by anterior half of somite 2, see Figure 2). There is no difference in axon targeting between WT siblings and *hox5* deficient embryos. WT sibs n = 10 embryos, *hoxa5a* n = 4, *hoxb5a* n = 4, *hoxb5b* n = 8, triple mutants n = 9. (I) Quantification of (C-G). There is no difference in axon targeting between WT siblings and *hox5* deficient embryos. WT sibs n = 10 embryos, *hoxa5a* n = 10, *hoxb5a* n = 7, *hoxb5b* n = 12, triple mutants n = 10. In (H,I) analysis done using Chi-square test comparing regions in pairwise combinations with respect to each axon branch. Regions

are considered different if they differ in at least one branch. Anterior is left and dorsal is up, and scale bars are 50 μm.

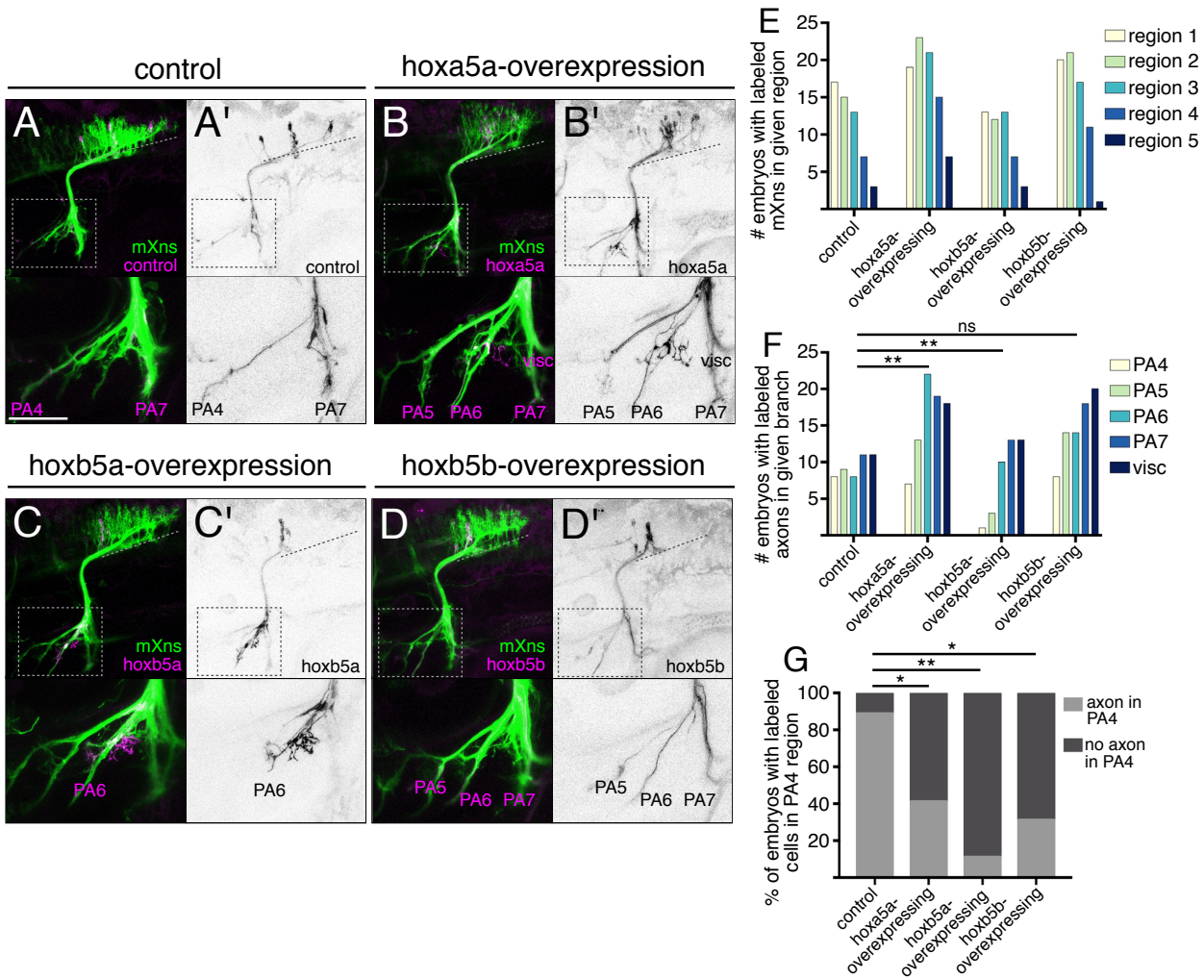

Figure 7. *hox5* expression directs mX axons to posterior targets.

(A-D) mX neurons expressing *hox5* genes are biased to innervate more posterior PAs. Expression of control *isl1:eGFPCAAX* (A) or *hox5*-ectopic expression construct (B-D) shown in magenta and (A'-D') black. All mX neurons express *Tg(isl1:mRFP)* (green). Dotted lines indicate length of mX territory, dotted boxes indicate region shown in bottom panels. (E) Quantification of distribution of labeled neurons in (A-D). Regions are based on morphological boundaries as in Figure S1. Distribution is not significantly different from control in any case. In both (E) and (F), control n = 17 embryos, *hoxa5a* n = 24, *hoxb5a* n = 20, *hoxb5b* n = 28. (F) Quantification of labeled axon targeting in (A-

D). Analysis was done using Fisher's exact test comparing control to each ectopic expression condition with respect to each axon branch. Conditions are considered different if they differ in at least one branch. (G) Analysis of axon targeting in (A-D) restricted to only those cases where a labeled mX neuron was located within the most anterior 20 μm of the mX territory (PA4 zone). Ectopic *hox5*-expressing mX neurons in the PA4 zone will not innervate PA4. Analysis done by Fisher's exact test comparing each *hox5* construct to control. Control n = 9 embryos, *hoxa5a* n = 17, *hoxb5a* n = 9 embryos, *hoxb5b* n = 16. Anterior is left and dorsal is up, and scale bars are 50 μm.

Chapter 4: Time of axon outgrowth instructs vagus topographic map development independently of *hox5* expression

Axon formation and arrival in the periphery is delayed in posterior mX neurons

In addition to *hox5* spatial patterning, the anterior-posterior sequence of PA innervation by mX neurons (Figure 1B,C, Movie 1,2) suggested there may be temporal differences between anterior and posterior mX neurons that impact axon targeting. We set out to characterize the temporal dynamics of anterior and posterior axon outgrowth by live imaging. To visualize behavior of individual neurons, we crossed the *Tg(isl1:Gal4)* line to the variegated *Tg(UAS:kaede)* line to mosaically label mX neurons, photoconverted posterior mX neurons, and imaged from 29 hpf. At this time point, early-born mX neurons are present throughout r8, and later-born neurons are seen undergoing their characteristic dorsal migration to join the mX nucleus (Ohata et al., 2009), but axons have only just begun to emerge (Figure 8A, Movie 3). Anterior mX axons exit the brain and turn ventrally to extend into the periphery at 29 hpf (95% confidence interval (CI) = 26.71-32.6 hpf), consistent with previous literature (Cox et al., 2011). However, posterior mX neurons that were also present and fully migrated at the beginning of the time lapse showed extensive protrusive activity but remained multipolar until axons were finally detected at 37.7±2.7 hpf (95% CI = 35.9-39.5 hpf), when anterior mX axons had already extended into the PAs (Figure 8A,B, Movie 3). Once present, posterior growth cones travel quickly, following tracts of previously extended anterior mX axons (Movie 3). This suggests that the delayed appearance of posterior mX axons is due to delayed axon initiation, rather than slow speed of travel in the fascicle.

One explanation for the observed delay in posterior mX axon formation could be that posterior mX neurons are born later than anterior ones. To test this possibility, we birthdated mX neurons with (2'S)-2'-deoxy-2'-fluoro-5-ethynyluridine (EdU). We added EdU to embryos carrying *Tg(isl1:GFP)* at 10, 14, 18, 22, or 28 hpf and fixed embryos at 48 hpf. We then identified mX neurons by GFP expression and determined whether each neuron underwent its last division before (EdU-) or after (EdU+) the time point at which EdU was added. We divided the mX territory into 5 equal sized regions and quantified the proportion of EdU-negative neurons in each region for each treatment time (Figure 8C,D). If time of axon formation correlates with time of birth, we would expect EdU-negative mX neurons to appear from anterior to posterior at progressively later EdU treatment times. However, this is not what we observed: postmitotic (EdU-) mX neurons appear at all anterior-posterior levels of the motor nucleus over a time period from 10 hpf-28 hpf, and there was no significant difference in the onset of neurogenesis between the five regions assayed (Figure 8E, p = ns by one-way ANOVA of all regions at 14 hpf). These results surprisingly show that the delayed onset of axon initiation of posterior mX neurons does not reflect a later birthdate, and suggests that timing of axon formation is an independently regulated event along the anterior-posterior axis of the vagus motor nucleus.

Vagus motor neuron position determines time of axon formation

Given that cell position correlates with time of axon formation, we sought to test whether cell position could determine time of axon formation. We therefore applied time lapse imaging to our postmitotic mX neuron transplant approach, where nascent

neurons were transplanted homotopically or heterotopically at 27 hpf. In control anterior → anterior transplants, mX neurons initiated axons 6.3±2.1 hours post transplantation (hpt) (95% CI = 5.1-7.5 hpt) (Figure 8F,J, Movie 4). However, transplanting mX neurons heterotopically from anterior → posterior delayed time of axon formation, with axons appearing 8.6±2 hpt (95% CI = 7.4-9.8 hpt) (Figure 8G,J, Movie 4, $p = 0.0067$ by unpaired t-test). Consistent with this result, in control posterior → posterior transplants, mX neurons initiated axons late (8.2±1.3 hpt, 95% CI = 6.9-9.6 hpt), while transplanting neurons heterotopically from posterior → anterior hastened time of axon formation (6.1±0.8hpt, 95% CI = 5.3-6.9 hpt) (Figure 8H-J, Movie 5, $p = 0.0051$ by unpaired t-test). These results suggest that cell position determines time of axon formation.

We noted that the difference in time of axon formation between the control and heterotopic transplants was smaller than that observed between endogenous anterior and posterior mX neurons (anterior → anterior versus anterior → posterior = 2.3 hour increase, posterior → posterior versus posterior → anterior = 2.1 hour decrease (Figure 8J), compared to the 8 hour difference between endogenous anterior and posterior mX neurons, Figure 8B). We suggest the primary reason for this discrepancy is that transplanted donor neurons require some amount of recovery time in the host before they are capable of extending axons. This is illustrated in anterior → anterior transplants, where donor-derived mX neurons initiate axons approximately 4 hours later than endogenous anterior mX neurons (33.8±2.5 hpf (95% CI = 32.6-35.1 hpf) vs. 29.7 hpf±1.9 hpf (95% CI = 26.7-32.6 hpf), $p = 0.0034$ by unpaired t test). This difference is less pronounced in posterior → posterior transplants where host axon initiation is

delayed and donor mX neurons therefore have time to recover (37.7±2.68 hpf (95% CI = 35.9-49.5 hpf) for donor-derived posterior neurons compared to 36.4± 2 hpf (95% CI = 34.4-38.5 hpf) for endogenous posterior neurons, p = ns by unpaired t test). Interestingly, the axon targeting of neurons transplanted to anterior r8 is less tightly restricted to PA4 than that of endogenous anterior mX neurons (compare Figure 3F to 1G), suggesting a delay in axon initiation of anterior mX neurons may affect mX axon targeting to anterior branches.

Time of axon arrival in the periphery determines axon targeting

Our transplant experiments demonstrated that mX neurons positioned in anterior r8 will initiate axon formation early (Figure 8) and will innervate anterior axon targets (Figure 3). Conversely, mX neurons positioned in posterior r8 will initiate axon formation late and will innervate posterior axon targets. We therefore sought to test the hypothesis that time of axon formation influences mX axon targeting. To do so, we simulated a delay in axon initiation by transplanting anterior mX neurons from a younger donor (25.9±2 hpf) to the anterior mX territory of an older host (31.8±2.1h hpf) such that the axon of the transplanted neuron joins the fascicle with late-arriving posterior mX axons (Figure 9A). If axon targeting is determined by anterior-posterior position alone, then we predicted that this heterochronically transplanted mX neuron will innervate anterior targets (PA4, PA5, or PA6). Alternatively, if timing of axon outgrowth influences axon targeting independently of position, then we predict that it will innervate a more posterior PA. We found that compared to stage-matched transplants, where donor-derived anterior mX neurons innervated primarily anterior PAs (Figures 3B, 9B,D), mX neurons

transplanted into older host embryos innervated primarily posterior PAs (Figure 9C,D). This change in axon targeting is not due to induction of ectopic *hox5* expression, because when we did the equivalent heterochronic transplant using our *hoxb5a*^{GFP} line as a donor, we did not see GFP expression in the transplanted neurons (Figure 9E,F). These results indicate that surprisingly, altering the temporal environment alone is sufficient to shift axon targeting, with donor neurons innervating posterior targets along with posterior mX axons.

The results from the heterochronic transplants show that axons that arrive at the choice point late are guided to more posterior targets. This suggests the possibility of axon-axon competition such that early-arriving anterior axons repel late-arriving axons, thereby restricting them to posterior branches as has been proposed for the mouse olfactory map (Takeuchi et al., 2010). To test this possibility, we laser-ablated anterior mX neurons at 35.5±1.5 hpf, a time point when anterior axons are extending into the periphery, but before posterior mX neurons have formed axons, and analyzed axon branch formation at 3 dpf (Figure 10A). We found that in 80% of ablated embryos, the anterior-most PA4 branch was absent, and in 70% of ablated embryos the anterior PA5 branch was thin compared to wild-type. Despite the lack of anterior branch formation, 100% of ablated embryos retained the posterior PA6, PA7, and visceral branches (Figure 10B, n = 10 embryos). These results suggest that early-arriving anterior mX axons do not compete with later-arriving posterior axons for innervation of PA4.

Hox5 expression and time of axon initiation direct mX axon targeting independently

Our experiments to this point demonstrated that the spatio-temporal environment of mX neurons influences their topographic mapping to the PAs. Position along the anterior-posterior axis of r8 determines *hox5* expression and time of axon formation, and both *hox5* expression and delayed axon initiation can target axons to more posterior PAs. We asked whether *hox5* expression is responsible for delayed axon initiation, which in turn drives posterior PA targeting, or whether the two are independent. If *hox5* expression delays axon initiation, we would expect that in our *hox5* ectopic expression approach, *hox5*-expressing mX neurons in the anterior mX territory would initiate axon formation late, at a time more appropriate for posterior mX neurons. We therefore imaged and quantified the time of axon formation in anterior *hox5*-expressing mX neurons. In this experiment, our time lapse movies ended at 2 dpf, preventing us from using our typical morphological boundaries to define anterior mX neurons. Here, we refer to an mX neuron as “anterior” if it was within the anterior-most quarter of the mX territory at the end of the time lapse. Control anterior mX neurons expressing *isl1:egfpCAAX* formed axons at 29.8±1.6 hpf (95% CI = 28.4-31.05 hpf), similar to the timing of anterior axon outgrowth determined by Kaede photoconversion (Figures 8A,B, 11A,E, Movies 3,6). Surprisingly, we observed no significant difference in the time of axon formation by anterior mX neurons expressing *hoxa5a*, *hoxb5a*, or *hoxb5b* compared to the control construct (Figure 11A-E, Movies 6-9). Together, these results indicate that delayed axon initiation guides axons to posterior targets

independently of *hox5* expression, and *hox5* expression guides axons to posterior targets independently of timing of axon initiation.

Summary: Delayed axon initiation and outgrowth in posterior mX neurons directs posterior axon targeting

In this chapter, we have shown through time lapse imaging and careful birthdating that axon initiation is delayed in posterior mX neurons independent of mX neuron birthdate. mX neurons that are either born in posterior r8 or transplanted into posterior r8 will initiate axon formation later than anterior mX neurons. This timing of axon outgrowth is important for axon targeting, as heterochronic transplants demonstrate that late axon growth into the periphery directs axons to posterior targets. Finally, we use time lapse imaging of ectopic *hox5*-expressing cells in anterior r8 to show that the time of axon initiation is independent of *hox5* expression.

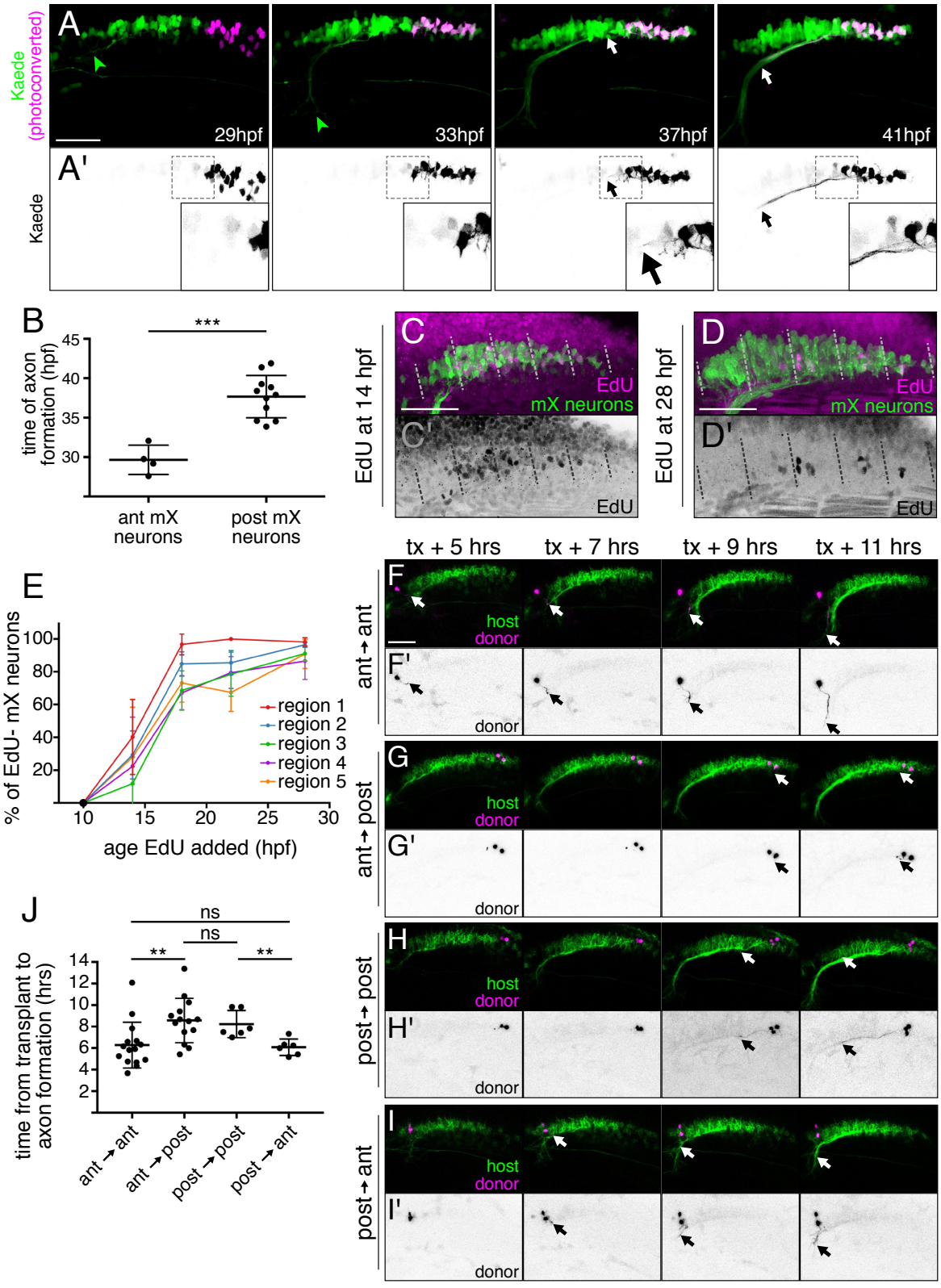

Figure 8. Time of axon formation and arrival in the head periphery is delayed in posterior mX neurons independently of birthdate.

(A) Stills from representative time lapse of embryo expressing *Tg(isl1:Gal4);Tg(UAS:kaede)* showing photoconverted posterior mX neurons in magenta (A) or black (A'). Axons of anterior mX neurons are detectable at 29 hpf, while posterior mX axons are not detectable until 37 hpf, though they show extensive multipolar protrusive activity. Green arrowhead indicates tip of anterior mX axons, white arrow indicates the growth cone of posterior mX axons. See also Movie 3. (B) Quantification of (A). Each point represents a single embryo. Analysis done by unpaired t test. (C,D) Embryo expressing *Tg(isl1:GFP)* to mark motor neurons (green) was incubated in EdU (magenta and (C',D') black) to label mX neurons born after 14 hpf (C) or 28 hpf (D). Embryos were fixed at 48 hpf and the mX territory was divided into 5 equal sized regions from anterior (1) to posterior (5). (E) Quantification of (C,D) showing percentage of postmitotic (EdU-) mX neurons in each region at each time point ([# EdU-GFP+ cells]/[# GFP+ cells]). Each point represents mean, error bars show standard deviation. At 10 hpf, 0% of mX neurons were EdU- for all regions (black circle). n = 5 embryos for all time points except 14 hpf, where n = 4 embryos. (F-I) Transplanting an anterior mX neuron into the posterior delays axon formation (F,G) while transplanting a posterior mX neuron into the anterior hastens axon formation (H,I). Donor neurons marked by *Tg(isl1:kaede)* in magenta and (F'-I') black, and host neurons marked by *Tg(isl1:mRFP)* in green. See also Movies 4,5. (J) Quantification of (F-I). Each point represents a single embryo. Analysis done by unpaired t test. Anterior is left and dorsal is up, and scale bars are 50 μm.

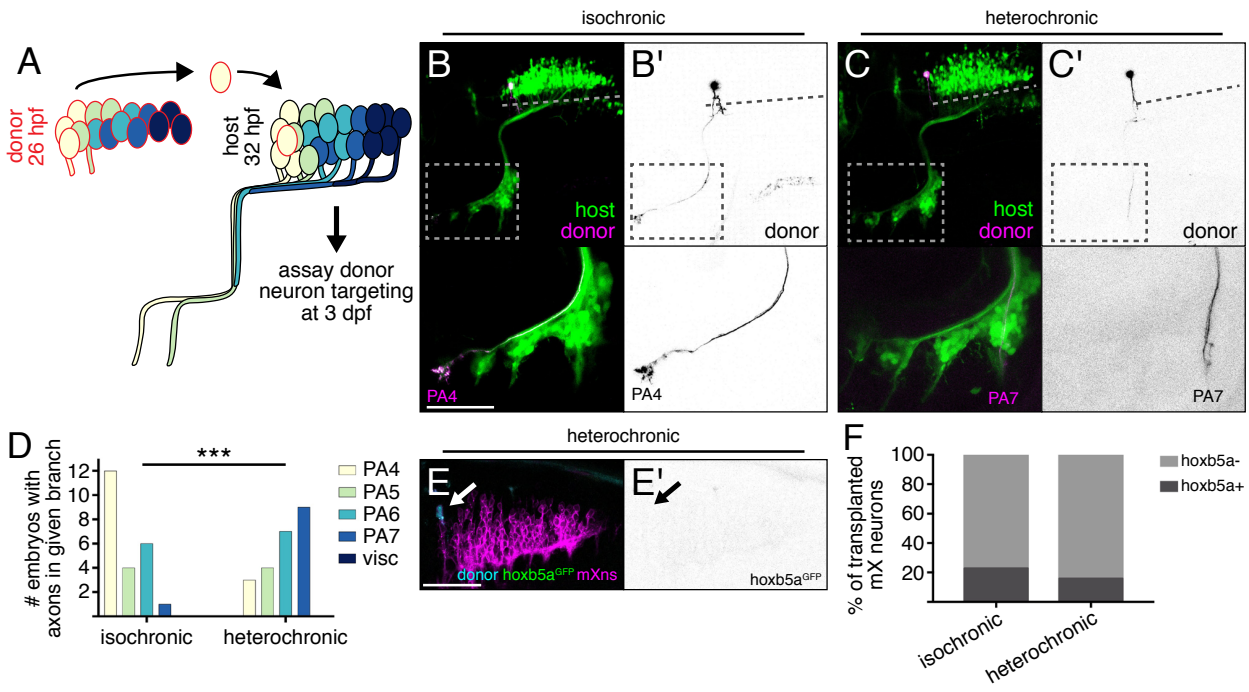

Figure 9. Time of mX axon outgrowth determines peripheral target independently of hox5 expression.

(A) Schematic of postmitotic neuron transplantation. mX neurons are transplanted heterochronically before axon formation, from anterior to anterior, and donor axon targeting is assayed at 3 dpf. (B,C) Anterior mX neurons transplanted isochronically (B) innervate anterior targets while anterior mX neurons transplanted heterochronically (C) innervate posterior targets. Images show donor axons, marked by *Tg(isl1:kaede)* in magenta and (B',C') black. Host motor neurons are marked by *Tg(isl1:GFP)* in green. Dotted lines indicate length of mX territory. Dotted boxes indicate region shown in bottom panels. (D) Quantification of transplant results showing number of host embryos with a donor axon in a given branch. Isochronic control transplants are the same data shown in Figure 3F (anterior → anterior). Analysis done using Fisher's exact test, see STAR Methods for details. Isochronic n = 14 host embryos, heterochronic n = 16. (E) Change in targeting after heterochronic transplantation is not due to induction of *hox5*

expression. Donor embryos carried *Tg(isl1:mRFP)* (magenta) and *hoxb5a*^{GFP} (green and (E') black) reporters and were injected with cascade blue vital dye (cyan). Host embryos carried only *Tg(isl1:mRFP)*. (F) Quantification of (E). Donor-derived motor neurons are identified by coexpression of cascade blue and *Tg(isl1:mRFP)*. Shown here is percentage of donor mX neurons expressing *hoxb5a*^{GFP}. Isochronic control transplants are the same data shown in Figure 5F. Heterochronic n = 19 cells, 11 embryos. Anterior is left and dorsal is up, and scale bars are 50 μm.

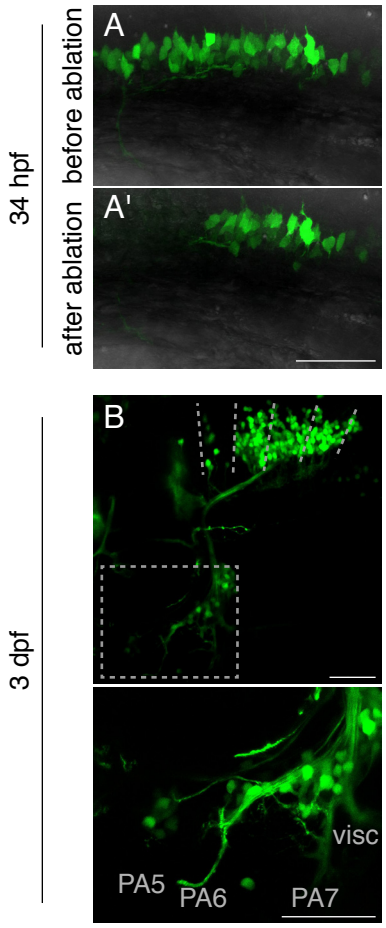

Figure 10. Ablation of anterior mX neurons does not affect posterior mX axon targeting.

(A) Anterior mX neurons were ablated before posterior mX neurons initiate axon formation in an embryo expressing *Tg(isl1:kaede)*. (B) Representative image of mX axon branches at 3 dpf in an ablated embryo. In 80% of ablated embryos, the PA4 branch was absent, and in 70% of ablated embryos, the PA5 branch was thin. n = 10 ablated embryos. Anterior is left and dorsal is up, and scale bars are 50 μm.

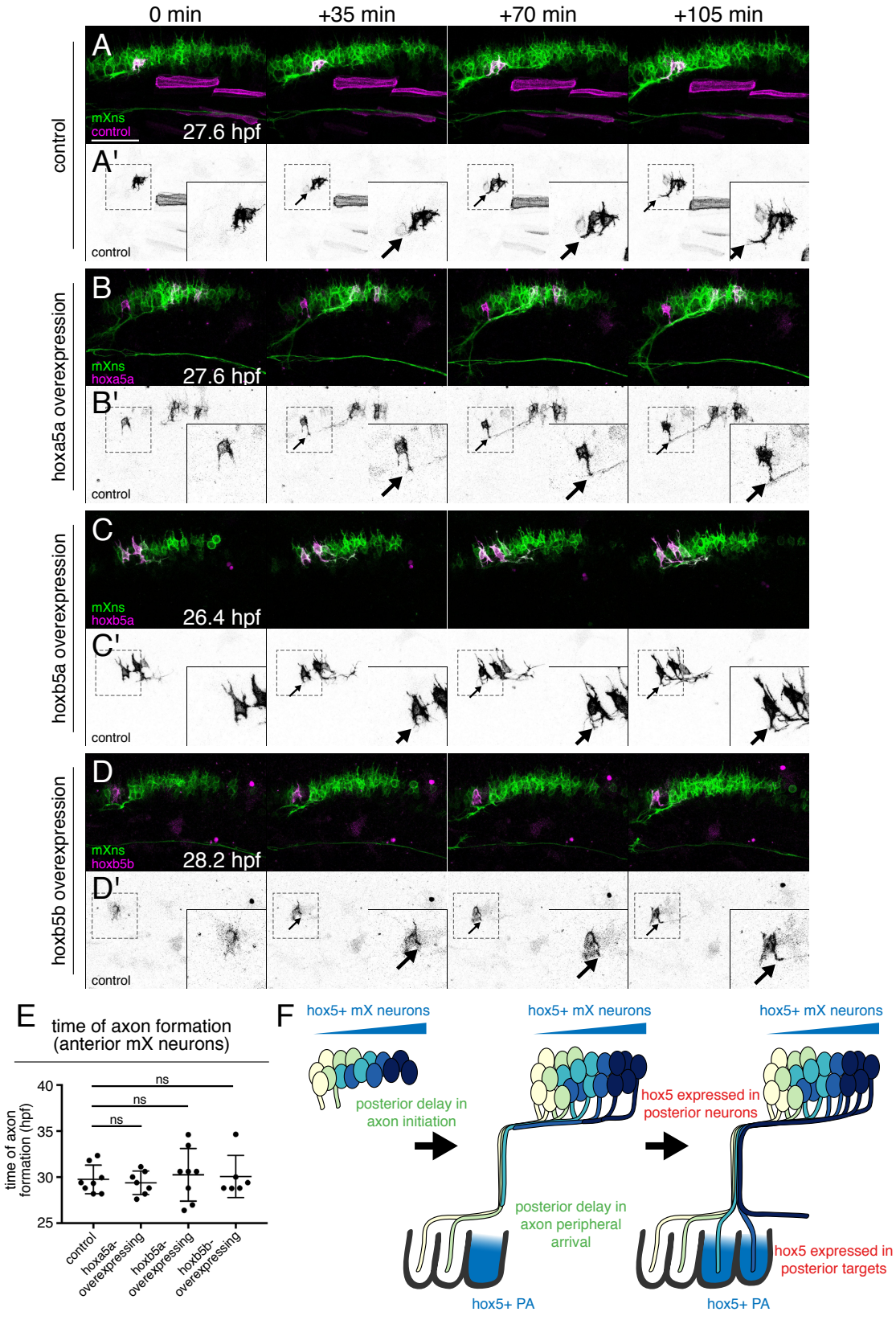

Figure 11. *hox5* acts independently of time of axon formation

(A-D) *hox5* expression does not change time of axon formation in anterior mX neurons. Stills from representative time lapse showing control or ectopic *hox5*-expressing neurons in magenta and (A'-D') black. All mX neurons marked by *Tg(isl1:mRFP)* (green). Arrows indicate the emerging axon. See also Movies 6-9. (E) Quantification of (A-D). Each point represents a single embryo. mX neurons included in this analysis were within the anterior-most quarter of the mX territory. Analysis done by unpaired t test. (F) Model of dual mechanisms governing mX neuron topographic map development. In a classic spatial patterning mechanism (red text), *hox5* genes are specifically expressed in posterior mX neurons and posterior PAs, and direct axons towards posterior targets. In a novel temporal mechanism (green text), axon initiation is delayed in posterior mX neurons, which then delays axon arrival in the periphery. Late-arriving axons are directed to posterior targets. Anterior is left and dorsal is up, and scale bars are 50 μm.

Chapter 5: Transcriptome analysis of anterior and posterior mX neurons

Single cell picking allows RNA isolation from anterior versus posterior mX neurons

Our results show that delayed axon initiation and *hox5* expression in posterior mX neurons underlies the development of the mX neuron topographic map. We next sought to determine the molecular mechanism underlying these processes: both to identify proteins regulating time of axon initiation and to identify *hox5* target genes controlling axon guidance. We reasoned that transcriptome analysis may allow us to accomplish both of these goals by comparing anterior and posterior mX neurons at a time when axon initiation has begun in anterior but not posterior mX neurons.

To selectively label either anterior or posterior mX neurons, we elected to use a photoconversion approach with the *Tg(isl1:Kaede)* line, as our *hoxb5a*^{GFP} reporter perdures and may not faithfully report *hox5* expression at a particular point in time (Figure 5B). At 28 hpf, when axons are just emerging from anterior mX neurons, we selectively photoconverted mX neurons in either the anterior-most quarter of the mX territory, which we know from *in situ* hybridization experiments to be *hox5-*, or mX neurons in the posterior-most quarter of the mX territory, which we know to be *hox5+* (Figures 4,5A). We then dissociated embryos into a single cell suspension and selected the appropriate mX neurons by picking only those cells that were expressing red (photoconverted) Kaede (Figure 12, see Materials & Methods for details). We collected 3 independent pools of 100 anterior mX neurons or 100 posterior mX neurons (Tables 1, 2). This approach is sufficient to identify genes differentially expressed in different

types of zebrafish pigment cells (L. Saunders & D. Parichy, personal communication). It is important to note that because cells aggregate quickly in suspension, our pools contained some cells that were not *Tg(isl1:kaede)*+ mX neurons, and could include other neurons, neural progenitors, or peripheral cell types that were included in the dissection of the r8 territory (Tables 1, 2). However, these were represented equally in both the anterior and posterior pools (Table 2), so while they may add non-motor neuron transcripts to the sequenced reads, they are not expected to interfere with the identification of differentially expressed genes. We isolated RNA from these 100-neuron samples and then worked in collaboration with the Genomics Core at Fred Hutch to prepare and sequence libraries from each sample. Our sequencing data identified 12327 genes that were differentially expressed in our anterior versus posterior samples, 12 of which passed our threshold of significant differential expression in anterior versus posterior mX neurons (Table 3, see Materials & Methods for details). This small number of significantly differentially expressed candidate genes is expected given that the cell types we are comparing—anterior versus posterior mX neurons—are so similar.

RNA-Seq dataset shows differential expression of *hox5* genes

Our previous RNA *in situ* hybridization and reporter lines clearly showed that *hox5* genes are expressed in posterior but not anterior mX neurons. Expression of *hox5* genes therefore provides an excellent internal control to validate our RNA-Seq dataset. Encouragingly, *hoxb5a* was one of four genes that were significantly enriched in posterior mX neurons (Table 3, average reads mapped in anterior = 645, average reads mapped in posterior = 5162, log2(fold change) = 3.2). Similarly, *hoxb5b* was enriched in

posterior mX neurons compared to anterior mX neurons, though it did not meet our threshold of significant enrichment (Table 3, average reads mapped in anterior = 10291, average reads mapped in posterior = 27464, log2(fold change) = 1.6). This indicates that our approach is capable of identifying genes that are differentially expressed between anterior and posterior mX neurons.

Unexpectedly, our filtering approach did not identify *hoxa5a* as a top candidate gene enriched in posterior mX neurons. This is likely due to the relatively low coverage of *hoxa5a* (average reads mapped in anterior = 361, average reads mapped in posterior = 1506, log2(fold change) = 2.25). Interestingly, although our RNA *in situ* hybridization results showed that *hoxc5a* was not expressed in rhombomere 8, our RNA-Seq results showed that expression of *hoxc5a* was similar to *hoxa5a* (averaged reads mapped in anterior = 653, average reads mapped in posterior = 1847, log2(fold change) = 1.7). This raises the possibility that our RNA *in situ* hybridization against *hoxc5a* may not have been sensitive enough to detect true expression. If *hoxc5a* is truly enriched in posterior mX neurons, it may contribute to guidance of posterior mX axons, suggesting the possibility that normal mX neuron map development in the *hox5* triple knockdown embryos is due to redundant function of *hoxc5a*. We may test this possibility in the future with a morpholino approach, co-injecting morpholinos against *hoxa5a* and *hoxc5a* into *hoxb5a;hoxb5b* double mutant embryos.

In addition to *hoxb5a* and *hoxb5b*, our sequencing also identified *hoxb6b* as a gene that is enriched in posterior mX neurons, though it did not meet the threshold for significance (Table 3, average reads mapped in anterior = 2780, average reads mapped

in posterior = 11875, log2(fold change) = 2.3). However, our previous RNA *in situ* hybridization experiments showed that *hoxb6b* is not expressed in the mX territory and only weakly expressed posterior to rhombomere 8. This indicates either that our RNA *in situ* hybridization probes were not sensitive enough to detect expression in posterior mX neurons, or that there may be false positive candidate genes returned in our RNA-Seq dataset. In either case, this underscores the need to validate all candidates either by RNA *in situ* hybridization on intact brains or qPCR of isolated mX neurons.

Identification of genes that are enriched in anterior mX neurons

While all candidate genes from the transcriptome dataset still require validation, it is interesting to examine the list and speculate about potential roles of candidate genes in mX neuron development. Our transcriptome dataset was generated at a time point when anterior but not posterior mX neurons have initiated axons. Therefore, genes that are enriched in anterior mX neurons compared to posterior mX neurons represent candidate genes that regulate axon specification and formation.

There were eight genes that were significantly enriched in anterior mX neurons. For the genes *focad*, *kdsr*, and *fsd1*, there is no expression data available in zebrafish embryos and little functional data in published literature, making it difficult to assess their viability as candidate genes in mX neuron development. We consider here those genes where there is expression or functional data available consistent with a differential role in mX neuron development.

Of the eight genes that were significantly enriched in anterior mX neurons, four of them encode for cytoskeletal-associated proteins: *inab*, *ndel1b*, *myo10*, and *kifc2* (Table

3). This agrees with our understanding of axon initiation, which necessarily involves significant reorganization of the cytoskeleton as one neurite becomes specified as an axon and rapidly elongated (Kapitein & Hoogenraad, 2015). Additionally, the ankyrin protein *ank2b* was enriched in anterior cells, thought it did not pass our threshold for significance (Table 3). The ankyrin proteins are a family of plasma membrane-organizing proteins that are important for axon elongation and especially for structural organization of the axon initial segment (Galiano et al., 2012; Hedstrom, Ogawa, & Rasband, 2008; Lorenzo et al., 2014; Qu et al., 2016). Expression patterns of *inab*, *myo10*, and *ank2b* in published literature confirms they are expressed in hindbrain motor neurons, though there is no differential expression detectable in r8 (Sittaramane & Chandrasekhar, 2008; Bernard Thisse & Thisse, 2004). *ndel1b* shows broad expression at 24 hpf (Bernard Thisse & Thisse, 2004), while there is no expression data available for *kifc2*.

There is additionally functional evidence to support the idea that these cytoskeletal proteins promote axon initiation in anterior mX neurons. *myo10*, for example, is an unconventional myosin that promotes filopodia formation (Zhang et al., 2004), and some isoforms promote axon elongation while others are required to stabilize microtubules during axon initiation (H. Yu et al., 2015). Morpholino experiments in zebrafish spinal neurons have shown that the neuronal intermediate filament protein *inab* is required for proper axon branching and morphology (Van Ryswyk, Simonson, & Eisen, 2014). Finally, *ndel1b* regulates dynein, localizes to the axon initial segment, and is important in preventing somatodendritic cargo from accessing the axon (Kuijpers et

al., 2016; Sasaki et al., 2000). The fact that we identified these cytoskeletal proteins important for axon initiation and outgrowth as differentially expressed in our RNA-Seq dataset is quite interesting, as it suggests that axon initiation is an event that can be transcriptionally regulated.

The final gene that was significantly enriched in anterior mX neurons was the retinoic acid binding protein *crabp1b*. Published expression patterns of *crabp1b* in 24 hpf zebrafish embryos are consistent with our RNA-Seq findings, showing that *crabp1b* is strongly expressed in r7 and the anterior mX region, with weaker expression in the mX territory and spinal cord (Liu et al., 2005). Precise boundaries of *crabp1b* expression relative to the mX territory will require validation with morphological boundaries or a motor neuron marker such as *tbx20*. Retinoic acid signaling is known to be important for patterning the anterior-posterior axis of the hindbrain, and indeed morpholino experiments in zebrafish embryos have shown that *crabp2a* and *crabp2b* are required for expression of *hoxb5* genes. Retinoic acid is typically thought of as a posteriorizing cue, and *crabp2* is known to interact with the retinoic acid receptor to enhance retinoic acid signaling (Delva et al., 1999; Jing, Waxman, & Mira-y-Lopez, 1997), making it curious that *crabp1b* is more highly expressed in anterior mX neurons. However, there is evidence that *crabp1* counteracts the effects of exogenous retinoic acid and enhances retinoic acid metabolism (Boylan & Gudas, 1991; Won et al., 2004). We therefore speculate that *crabp1b* may be important for decreasing retinoic acid sensitivity in anterior mX neurons.

In addition, there were homologs of several intriguing genes known to be involved in axon biology that were enriched in anterior mX neurons, though they did not pass our threshold for significant enrichment, including *olfm2a*, *npr2b*, *ptprfa*, and *rnd3a*. *olfm2a* belongs to a family of secreted glycoproteins that have broad and diverse effects in the nervous system (Lee, Anholt, & Cole, 2008). *olfm2a* in particular is expressed in hindbrain motor neurons (Bernard Thisse & Thisse, 2004), and interestingly, knockdown of *olfm2a* with morpholinos in zebrafish embryos leads to defects in cranial motor axon guidance, including in mX neurons. mX axons are still present, arguing against the idea that *olfm2a* is required for axon initiation, but there are peripheral guidance defects in morphant embryos including failure of mX neurons to innervate the PAs. Intriguingly, morphant embryos show complete absence of the PA4, PA5, and PA6 branches, while the PA7 and visceral branches were present, albeit with thin fascicles and guidance defects. This supports the idea that *olfm2a* may be selectively influencing guidance of anterior mX axons. However, it is unclear how a secreted protein expressed in motor neurons would affect mX axon guidance.

There were also two interesting receptors that were enriched in anterior mX neurons, *ptprfa* and *nrp2b*. Both are expressed in hindbrain motor neurons, though a graded expression pattern in r8 has not been described (F. Wang, Wolfson, Gharib, & Sagasti, 2012; H.-H. Yu, Houart, & Moens, 2004). *nrp2b* is a receptor for the *semaphorin3* axon guidance molecule, and our lab has previously demonstrated a role for *nrp2b* in cranial neural crest migration. However, a role for *nrp2b* in mX neuron topographic map development has not been explored. The receptor *ptpfra* has

intriguingly been shown to promote neurite outgrowth in cultured mouse hippocampal neurons (Yang, Yin, Derevyanny, Moore, & Longo, 2005), suggesting the interesting though speculative possibility that *ptpfra* promotes neurite outgrowth in anterior mX neurons to promote axon initiation.

Finally, the Rho family member *rnd3a* is an interesting hit from our RNA-Seq dataset, as hippocampal neurons cultured from mice lacking *Rnd3* show delayed axon initiation and reduced axon outgrowth (Peris et al., 2012). Published expression patterns of *rnd3a* in zebrafish embryos show that it is expressed in the hindbrain at 24 hpf with stronger expression in the anterior hindbrain, consistent with our RNA-Seq data (Kudoh et al., 2001). This suggests the possibility that *rnd3a* promotes axon initiation in anterior mX neurons.

Identification of genes that are enriched in posterior mX neurons

Candidate genes that are enriched in posterior mX neurons compared to anterior mX neurons may be involved in delaying axon initiation in posterior mX neurons, or may represent *hox5* target genes important for posterior axon targeting. Four genes were significantly enriched in posterior mX neurons, including *hoxb5a* as discussed above. The list also included another *hox* gene, *hoxb1b* (Table 3). *hoxb1b* is expressed in the hindbrain with an anterior expression boundary at r3 (McClintock, Carlson, Mann, & Prince, 2001), and though differential expression in rhombomere 8 has not been specifically explored, RNA *in situ* hybridization images from previous literature do show a graded expression pattern with higher levels in the posterior hindbrain (B. Thisse et al., 2001). Consistent with anterior hindbrain expression, previous work from our lab has

shown that mutations in *hoxb1b* lead to defects in neural tube morphogenesis in r3 and r4 due to misorientation of the mitotic spindle in neural progenitors (Zigman, Laumann-Lipp, Titus, Postlethwait, & Moens, 2014). We have not yet explored whether the mX neuron map is affected in *hoxb1b* mutants.

Additional candidate genes that were significantly enriched in posterior mX neurons included *drgx* and *dhrs3b*. *drgx* is a homeobox transcription factor that is expressed in cranial sensory neurons, including the vagal sensory ganglia, but is clearly not expressed in mX neurons by RNA *in situ* hybridization at 24 hpf (Dyer, Linker, Graham, & Knight, 2014). We therefore consider *drgx* a false positive hit. *dhrs3b* is a dehydrogenase/reductase enzyme involved in retinoic acid signaling. Expression patterns in zebrafish embryos at 24 hpf show that *dhrs3b* is expressed in the posterior but not anterior hindbrain, although the low resolution of the images makes it difficult to determine where the boundaries of *dhrs3b* expression are relative to r8. In *Xenopus* animal cap explant studies, expression of *dhrs3* is induced by addition of retinoic acid (Kam et al., 2013). Retinoic acid is well-known for its role in induction of *hox* gene expression in the posterior hindbrain, and interestingly, the expression pattern of *dhrs3b* in zebrafish embryos is similar to the *hoxb5a* expression pattern not just in the hindbrain but also in the tailbud (B. Thisse et al., 2001). This suggests the intriguing, though entirely speculative, possibility that *dhrs3b* is a downstream target of *hox5* genes. Future work will address this possibility by assessing *dhrs3b* expression in *hox5* triple knockdown animals.

Summary: Differential gene expression in anterior versus posterior mX neurons

We used a low input RNA-Seq approach to generate transcriptome datasets for anterior versus posterior mX neurons at a time when anterior but not posterior mX neurons have begun the process of axon initiation. Our analysis identified *hoxb5a* as a gene that was significantly enriched in posterior mX neurons, confirming the ability of this approach to identify genes that are differentially expressed within r8. Though there is much future work to be done in validating candidate genes and exploring their contribution to mX neuron topographic map development, this dataset represents an important and promising step forward in identifying additional genes that direct mX axon targeting.

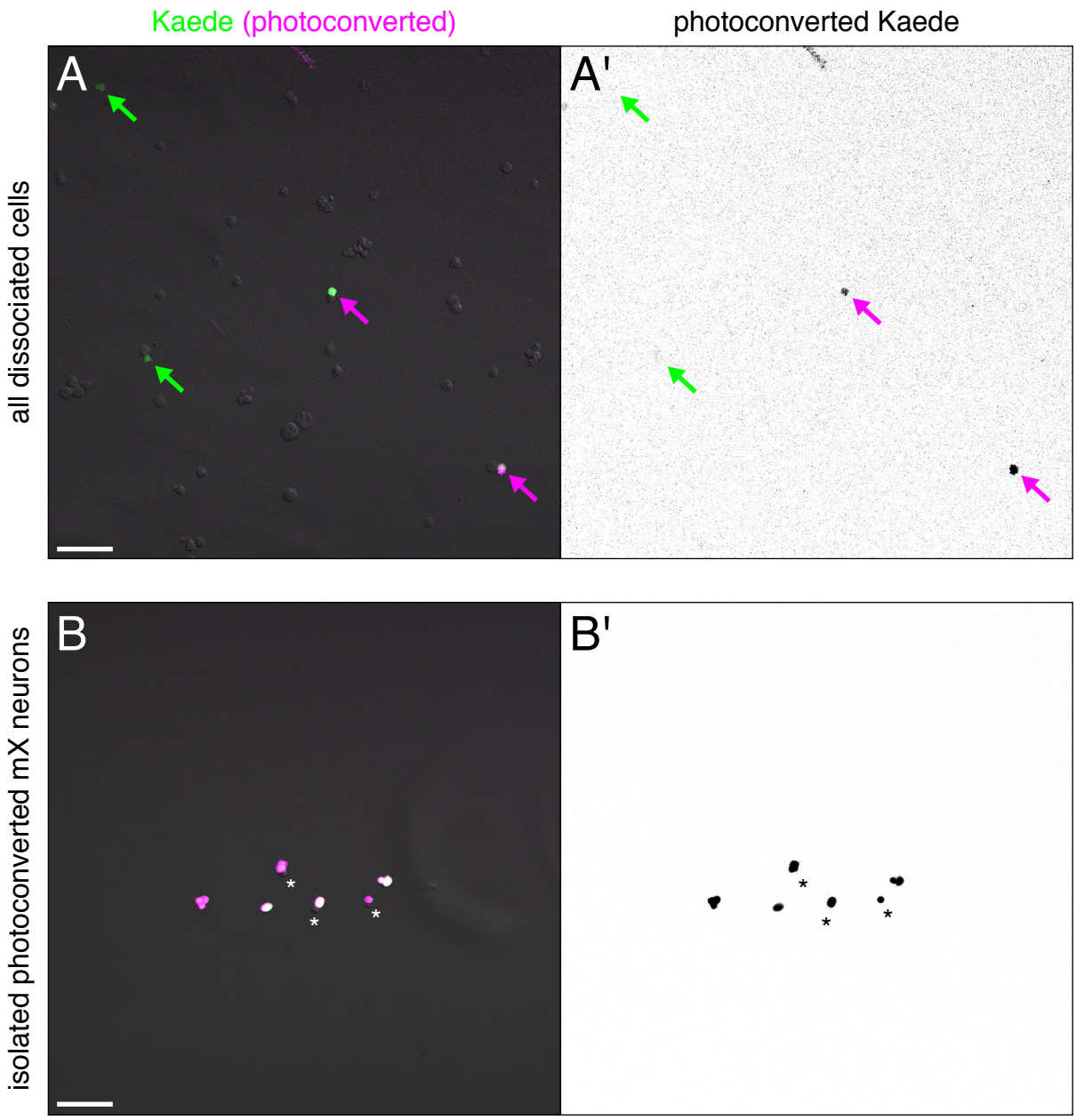

Figure 12. Cell picking for RNA isolation.

(A) Cells after rhombomere 8 dissociation. The suspension contains primarily *Tg(isl1:Kaede)*-negative cells, with occasional *Tg(isl1:Kaede)*-positive cells that were either photoconverted (magenta and (A') black, marked by magenta arrows) or not photoconverted (green, marked by green arrows). (B) mX neurons that have been selectively isolated by our single cell picking methods. Because our suspension did not

yield a complete single cell suspension, our same includes a small fraction of cells that are *Tg(isl1:Kaede)*-negative (marked by asterisks).

Table 1. Individual tubes for RNA isolation.

We collected either anterior or posterior mX neurons for RNA isolation. "# red cells" indicates the number of photoconverted mX neurons in a single tube, "# additional cells" indicates the number of additional *Tg(isl1:Kaede)*-negative cells added to that tube. Color shading indicates which sample each tube was added to (green, red, or blue).

date cells picked	cell type	# red cells	# additional cells
9/6/16	anterior	72	0
9/8/16	anterior	40	0
12/21/16	anterior	13	10
12/21/16	anterior	15	17
1/5/17	anterior	14	13
1/5/17	anterior	19	18
3/6/17	anterior	18	6
4/4/17	anterior	15	11
4/4/17	anterior	20	12
4/4/17	anterior	22	16
4/20/17	anterior	21	2
4/20/17	anterior	13	3
4/20/17	anterior	16	3
9/8/16	posterior	40	0
9/13/16	posterior	6	0
9/15/16	posterior	50	0
3/6/17	posterior	9	6
3/6/17	posterior	30	14
3/6/17	posterior	25	11
3/14/17	posterior	4	1
3/14/17	posterior	22	10
3/14/17	posterior	25	14
3/14/17	posterior	21	5
4/6/17	posterior	14	10
4/6/17	posterior	10	8
4/6/17	posterior	22	14
4/6/17	posterior	21	5

Table 2. Samples used for RNA isolation and sequencing.

Individual tubes were combined into 3 replicates each of anterior and posterior mX neurons for RNA isolation and sequencing. “total # mX neurons” indicates the total number of mX neurons that were combined in each sample, “total # additional cells” indicates the number of additional *Tg(isl1:Kaede)*-negative cells included in each sample.

sample name	abbreviation	total # mX neurons	total # additional cells
anterior green	AG	99	16
anterior red	AR	100	32
anterior blue	AB	99	63
posterior green	PG	101	27
posterior red	PR	98	51
posterior blue	PB	100	20

Table 3. List of selected genes that are differentially expressed between anterior and posterior mX neurons.

Light blue shading indicates gene is enriched in anterior mX neurons, while dark blue shading indicates gene is enriched in posterior mX neurons. Significance of 1 indicates the gene passed our threshold to be considered significantly differentially expressed in anterior versus posterior mX neurons (see Materials & Methods for details).

Gene	Full Name	log2(foldchange)	sig
drgx	dorsal root ganglia homeobox	11.32045739	1
inab	internexin neuronal intermediate filament protein, alpha b	-13.47346189	1
hoxb1b	homeobox B1b	3.173090963	1
ndel1b	nudE neurodevelopment protein 1-like 1b	-13.24468648	1
myo10	myosin X	-11.23132436	1
hoxb5a	homeobox B5a	3.169885337	1
crabp1b	cellular retinoic acid binding protein 1b	-3.229310165	1
focad	focadhesin	-12.95285694	1
kdsr	3-ketodihydrosphingosine reductase	-12.89459614	1
dhrs3b	dehydrogenase/reductase (SDR family) member 3b	2.495997484	1
fsd1	fibronectin type III and SPRY domain containing 1	-12.85150793	1
KIFC2	kinesin family member C2	-12.75539593	1
hoxb6b	homeobox B6b	2.283029105	0
dact2	dishevelled-binding antagonist of beta-catenin 2	12.54500949	0
scn8ab	sodium channel, voltage gated, type VIII, alpha subunit b	-12.61766564	0
plcxd3	phosphatidylinositol-specific phospholipase C, X domain containing 3	-2.739411397	0
nat10	N-acetyltransferase 10	-9.261878611	0
rnd3a	Rho family GTPase 3a	-1.969558524	0
itga5	integrin, alpha 5 (fibronectin receptor, alpha polypeptide)	-7.708768005	0
olfm2a	olfactomedin 2a	-2.797765957	0
ank2b	ankyrin 2b, neuronal	-2.286114479	0
shdb	Src homology 2 domain containing transforming protein D, b	2.040088114	0
neurod4	neuronal differentiation 4	1.614264058	0
itga3a	integrin, alpha 3a	-12.15751414	0
wbp2	WW domain binding protein 2	-12.15464979	0
hoxb5b	homeobox B5b	1.587450808	0
ptprfa	protein tyrosine phosphatase, receptor type, f, a	-2.663888324	0
nrp2b	neuropilin 2b	-2.172563588	0

Chapter 6: Conclusions and Future Directions

Topographic maps are of high interest to neurobiologists given their functional importance and prevalence throughout the central nervous system (Cang & Feldheim, 2013; Karmakar et al., 2017). Here, we further understanding of topographic map development by characterizing the vagus motor neuron topographic map in the larval zebrafish and presenting two mechanisms that function in parallel to govern its development. We demonstrate that *hox5* gene expression in posterior mX neurons drives posterior axon targeting in a spatial patterning mechanism. Second, we introduce a novel mechanism of topographic map development dependent upon delayed axon formation and outgrowth in posterior mX neurons (Figure 11F). Together, these dual mechanisms establish the complexity of the vagus motor neuron topographic map.

Hox5 expression drives posterior axon targeting

A major finding from our work is that *hox5* genes are expressed in posterior mX neurons and posterior PAs, and that *hox5* genes can direct posterior mX axons to posterior targets. *Hox* transcription factors are known to play roles in specifying neuron identity and axon targeting (Philippidou & Dasen, 2013) and to function in topographic map development in both motor and sensory systems (Dasen, Liu, & Jessell, 2003; Dasen et al., 2005; Oury et al., 2006). In cranial motor neurons specifically, *Hox* genes have previously been shown to be important for matching rhombomere identity and PA innervation. Neural crest cells that populate each PA are derived from the same rhombomere as neurons innervating that PA (Guthrie, 2007). For example, facial motor neurons are born in r4 and innervate PA2, and *Hoxb1* is expressed in both r4

neuroepithelial cells and PA2 neural crest cells. Deletion of *Hoxb1* from neural crest cells in PA2 leads to failure of innervation from r4-derived neurons (Arenkiel, Gaufo, & Capecchi, 2003), and ectopic expression of *Hoxb1* in r2 transforms r2 identity such that r2-derived neurons innervate PA2 (Bell, Wingate, & Lumsden, 1999). This is reminiscent of our results, where ectopic expression of *hox5* genes in mX neurons directs axon targeting towards targets normally innervated by *hox5+* mX neurons.

Hox genes affect axon targeting through both intermediate transcription factors and direct regulation of cell-surface guidance and adhesion molecules (Philippidou & Dasen, 2013). For example, *Hoxc6* in limb-innervating motor neurons induces expression of the transcription factor *FoxP1*, and *FoxP1* is required for the expression of axon guidance receptors including EphA4, which directs guidance of dorsal-limb innervating neurons by mediating repulsion from ephrinAs expressed in the ventral limb (Dasen, De Camilli, Wang, Tucker, & Jessell, 2008; Kania & Jessell, 2003). In cerebellar pontine neurons, *Hoxa2* and *Hoxb2* are required for migration along the anterior-posterior axis, in part through direct regulation of *Robo2* expression, which mediates repulsion from Slit2/3 expressing neurons in the facial motor nucleus to prevent premature ventral migration (Geisen et al., 2008). However, in our system, *hox5* target genes that direct targeting of posterior mX neurons remain unknown.

Given the expression of *hoxb5a* in both the posterior mX neurons and their target region, an intriguing possibility is that *hox5* acts through regulation of a homophilic adhesion molecule. In the chick, *Hoxb1* expression in r4 and PA2 induces expression of the leucine-rich repeat protein Lrrn2, and ectopic Lrrn2 expression in r2 leads to

misrouting of r2 axons into PA2 (Andreae, Lumsden, & Gilthorpe, 2009), suggesting a homophilic matching system may also be present downstream of *hox5* in our system. Homophilic cadherin interactions have also been shown to affect connectivity of both photoreceptors and lamina neurons in the *Drosophila* visual system, which extend axons into the layered structure of the medulla (Nern, Zhu, & Zipursky, 2008; Petrovic & Hummel, 2008). In the case of the R7 and R8 photoreceptors, cadherin-N is expressed in both R7 and R8 as well as their individual targets. Temporal regulation of the transcription factor *sequoia* in R7 and R8 is thought to mediate competence to respond to the ubiquitously expressed cadherin-N, as loss of cadherin-N suppresses the *sequoia* mutant targeting phenotype (Petrovic & Hummel, 2008). Therefore, though this provides precedent for homophilic adhesion molecules in axon targeting, it is unique from the *hox5* matching system we propose where a homophilic adhesion molecule may be expressed only in a subset of neurons and targets. In vertebrates, cadherins also affect axon targeting decisions in the visual system, where *cadherin8* and *cadherin9* are expressed by 2 types of retinal bipolar cells and required in the bipolar cells for proper laminar targeting in the retina. However, in that system, cadherins are thought to act heterophilically, as ectopic expression of *cadherin8* or *cadherin9* is sufficient to redirect targeting of bipolar cells in a *cadherin* mutant mouse (Duan, Krishnaswamy, De la Huerta, & Sanes, 2014).

An important goal of future experiments will be to identify genes that direct posterior mX axon targeting downstream of *hox5*. Our RNA-Seq experiment to compare transcriptomes of anterior and posterior mX neurons represents an important step

forward towards this goal. Transcriptomes were isolated at a time point when *hox5* genes are expressed in posterior mX neurons, so we may expect that *hox5* target genes would also be present in the posterior but not anterior mX neuron transcriptome. We have already begun to identify genes that are selectively expressed in posterior mX neurons. Our immediate goal is to verify differential expression using RNA *in situ* hybridization. We will then determine whether expression of candidate genes is under the control *hox5* transcription factors by assaying gene expression via RNA *in situ* hybridization in *hox5* triple knockdown embryos. We will then test the contribution of these candidate genes to mX axon targeting via both loss-of-function and gain-of-function approaches.

Time of axon initiation is regulated independently of birth order

A second major finding from our work is that axon initiation is delayed in posterior mX neurons despite the fact that anterior and posterior mX neurons have similar birthdates, and that this difference in timing plays a critical role in the formation of the topographic map. Timing of axon outgrowth has been previously proposed as a mechanism directing axon targeting. In the retinal ganglion cells of the mouse, differential timing of axon outgrowth correlates with axon targeting to different regions of the brain. However, this example remains correlative, as the authors did not have a means of altering time of axon outgrowth (Osterhout, El-Danaf, Nguyen, & Huberman, 2014). As described in Chapter 1, the *Drosophila* photoreceptor map and mouse olfactory map have similarly shown correlation between time of axon outgrowth and topographic axon targeting (Petrovic & Hummel, 2008; Takeuchi et al., 2010). However,

in these cases, it has not been possible to alter timing of axon outgrowth alone and assay for topographic wiring defects. Furthermore, in these examples differences in neuron birthdate underlie differences in timing of axon formation (Eerdunfu et al., 2017; Kulkarni et al., 2016; Petrovic & Hummel, 2008). Finally, in the frog retinotectal map, heterochronic transplantation was used to alter time of axon outgrowth, and timing of axon outgrowth was found not to affect topographic axon targeting (Holt, 1984). Our system is the first we are aware of where topographic mapping depends on the timing of axon outgrowth independently of neuron birthdate.

This raises the question of how timing of axon initiation is controlled in mX neurons. Axon initiation is a complex process that has been historically studied in cultured hippocampal neurons *in vitro* (Polleux & Snider, 2010). Once plated, neurons go through a series of defined stages beginning with initial immature filopodial and lamellipodial protrusions and progressing to multiple neurites that are arranged around the neuron in a multipolar organization (Dotti, Sullivan, & Banker, 1988). Polarity breaks when one neuron is specified as an axon, noted by the protrusion growing quickly away from the cell body, as well as early axon markers such as the microtubule binding protein TRIM46 (Dotti et al., 1988; Van Beuningen et al., 2015; van Beuningen & Hoogenraad, 2016). Both axons and dendrites then undergo maturation steps including branching, dendritic spine formation, and construction of the axon initial segment (Dotti et al., 1988; van Beuningen & Hoogenraad, 2016).

In vivo, axon initiation can vary between neuron types. Some neurons inherit polarity information from progenitor cells, as is the case for retinal ganglion cells in the

zebrafish (Morgan, Dhingra, Vardi, & Wong, 2006; Zolessi, Poggi, Wilkinson, Chien, & Harris, 2006). Live imaging of these neurons shows that there is no multipolar stage, but instead after the final division at the apical surface of the neuroepithelium, the basal process of the cell extends as an axon. Furthermore, apical processes retain apical markers including Par3, aPKC, a-catenin, and F-actin, indicating the neuron never experiences an unpolarized stage (Zolessi et al., 2006). Other neurons, including cortical neurons, adopt a multipolar morphology during migration before transitioning to a bipolar morphology, following which one neurite, typically the trailing process, is specified as an axon (Hatanaka & Yamauchi, 2013; Namba et al., 2014; Noctor, Martínez-Cerdeño, Ivic, & Kriegstein, 2004).

Many studies of axon initiation both *in vitro* and *in vivo* have elucidated intracellular signaling pathways, including Par proteins and their mammalian orthologs, that ultimately result in localized microtubule stabilization to specify one neurite as the future axon (Barnes et al., 2007; Chen et al., 2013; Kishi, Pan, Crump, & Sanes, 2005; Shelly, Cancedda, Heilshorn, Sumbre, & Poo, 2007; Shi, Jan, & Jan, 2003; Van Beuningen et al., 2015; Witte, Neukirchen, & Bradke, 2008; Yau et al., 2014). These cell-autonomous events can be biased by localized extracellular cues, including diffusible signaling molecules such as BDNF and TGF-beta, as well as contact-mediated cues in the neuronal microenvironment, such as laminin or TAG-1 on pioneer axons (Namba et al., 2014; Randlett, Poggi, Zolessi, & Harris, 2011; Shelly et al., 2007; Yi, Barnes, Hand, Polleux, & Ehlers, 2010).

In our system, we see that both anterior and posterior mX neurons complete their dorsal migration and exhibit extensive multipolar protrusions before axon formation. The multipolar morphology is reminiscent of cortical neurons before axon formation, but unlike cortical neurons, mX neurons do not adopt a bipolar morphology during migration. We think it likely that after completing migration, posterior mX neurons remain in a multipolar state longer than anterior mX neurons. Our transplant experiments suggest that the difference in axon initiation between anterior and posterior mX neurons is most likely due to a localized non-cell autonomous cue that either promotes axon initiation in anterior mX neurons, similar to BDNF and TGF-beta signaling in mammalian hippocampal and cortical neurons (Shelly et al., 2007; Yi et al., 2010), or prevents axon initiation in posterior mX neurons, similar to the role of Semaphorin3A in rat cortical neurons (Shelly et al., 2011).

Determining the nature of an extracellular cue that regulates time of axon initiation is an important goal for future work. Our experiment to compare the transcriptomes of anterior and posterior mX neurons identified cytoskeletal regulators that may be important for axon initiation, but was not designed to identify an extracellular cue. However, we did identify the receptors *ptprfa* and *nrp2b* as enriched in anterior mX neurons, suggesting their respective ligands Heparan Sulfate Proteoglycans or Semaphorin3s may act as extracellular cues to direct axon initiation. In future work, we will test the contribution of these candidate genes to axon initiation through loss-of-function and gain-of-function approaches.

Late axon arrival in the periphery drives posterior axon targeting

Posterior mX axons arrive in the periphery later than anterior mX axons due to the delay in axon initiation. Our heterochronic transplant experiments demonstrate that late-arriving axons are guided to posterior targets, but how this guidance occurs is unclear. We considered the possibility that late-arriving axons are restricted to posterior PAs through the action of early-arriving anterior axons, as axon-axon competition is important for retinal topographic map refinement in some species (Brown, Patel, Brzezinski, & Glaser, 2001; J. W. Triplett et al., 2011). However, our ablation experiments showed that PA4 is not innervated in the absence of anterior mX neurons, arguing that posterior mX axons are not restricted to posterior PAs by the presence of anterior mX axons in anterior PAs. Therefore, we consider it more likely that sequential innervation of the PAs over time is regulated by an attractive guidance cue that is temporally expressed in each PA such that each PA is only competent for innervation during a short time window. It is well established that PAs develop in an anterior-posterior sequence (Schilling & Kimmel, 1997). Therefore, it is possible that the temporally regulated mX axon initiation we discovered is dependent on the sequential development of the PAs.

The best candidate for a PA-derived mX guidance cue is HGF, which is expressed in the PAs and signals through the Met receptor on cranial motor axons, acting as a chemoattractant (Caton et al., 2000). In future experiments, we and other lab members will first perform a time course of *hgfa* and *hgfb* expression in the PAs to determine if it is sequentially expressed in the PAs as our model predicts. We will first

use RNA *in situ* hybridization to characterize expression of *hgfa* and *hgfb*, and we will then visualize *hgf* expression at high resolution in live embryos by using a CRISPR-Cas9 approach to create a reporter of *hgfa* or *hgfb* expression as we did for *hoxb5a*. In this case, it will be crucial to characterize the precise timing of *hgf* expression in the PAs relative to time of mX axon growth, so we will modify our existing plasmid with a fast-folding SYFPCAAX ((Paré et al., 2014) and Athea Vichas) or destabilized GFP or YFP (Ninov, Borius, & Stainier, 2012) to eliminate the problem of GFP perdurance. To determine if and how HGF-Met signaling is important for mX neuron topographic map development, we will also take advantage of an existing *met* loss-of-function mutant (Anderson et al., 2013) and create loss-of-function alleles for *hgfa* and *hgfb*, and assay effects on mX axon outgrowth and topographic mapping. If HGF-Met signaling is required for proper temporal innervation of the PAs, then we may see topographic mapping defects in a *met* or *hgf* mutant, with anterior mX neurons innervating posterior mX neurons, and vice versa. However, it is possible that we may see an intact mX neuron topographic map in the mutant embryo because the *hox5*-dependent mechanism is intact. In this case, we will combine the *hox5* mutant allele with the *met* or *hgf* mutant alleles. It is also possible that in *met* or *hgf* mutants, mX neurons fail to innervate the PAs entirely. If this is the case, we may test the effect of HGF on mX axon targeting using a bead implantation approach to induce exogenous HGF signaling. Implantation of gel beads ~100 μm in diameter into zebrafish PAs has been shown to successfully alter PA signaling (Holzschuh et al., 2005; Sperber & Dawid, 2008; Wiweger, Zhao, van Merkesteyn, Roehl, & Hogendoorn, 2012) and HGF-coated beads

are known to induce Met-dependent axon growth in chick explants (Guthrie & Lumsden, 1992). Zebrafish PAs are ~50 μm wide (Figure 1A), so careful implantation of an HGF-coated bead may be able to induce ectopic HGF signaling in PA6 and PA7. We predict that implantation of HGF beads into posterior PAs at or before the time of anterior mX axon outgrowth will lead to topographic mapping defects with anterior mX neurons innervating both anterior and posterior PAs.

Temporal and spatial mechanisms act in parallel to direct topographic map development

Our heterochronic transplants demonstrate that time of axon outgrowth determines mX axon target independently of *hox5* expression, and our ectopic expression experiments demonstrate that *hox5* expression directs mX axons to posterior targets independently of time of axon outgrowth. This raises the question of how these two mechanisms work together to regulate map development. One possibility is that both mechanisms are required to achieve the complexity seen in the mX neuron map. The *hox5* genes divide the mX territory into two regions, which cannot not be sufficient to specify all five peripheral branches. Additionally, our time lapse experiments demonstrate that the timing of the visceral branch is uncoupled from the timing of the PA branches, suggesting that the timing mechanism may be more important for PA than visceral mX neurons.

Alternatively, these may be partially redundant mechanisms acting in parallel in a "belt-and-suspenders" manner to establish fidelity of axon targeting. Timing of mX axon outgrowth could direct initial targeting of axons to PAs that are accessible at the time

axons reach the periphery, and a *hox5*-dependent mechanism could act to prevent mismatches such that axons of *hox5*+ mX neurons do not innervate anterior (*hox5*-) PAs. If this is the case, one would not expect to see topographic mapping defects in a *hox5* mutant where *hox5* is absent from all mX neurons and PAs, consistent with our results in the *hox5* triple mutant. Furthermore, we noted that in our heterochronic transplants, mapping defects were weaker than expected: 25% of host embryos had donor axons exclusively in posterior branches and 31% of host embryos had donor axons in both anterior and posterior branches, compared to stage-matched anterior → posterior transplants, where transplantation alters both *hox5* expression and time of axon formation. In those transplants, 75% of host embryos had donor axons exclusively in posterior branches and only 8% of host embryos had donor axons in both anterior and posterior branches. Perhaps the relatively mild posterior targeting in this case is because the *hox5* mechanism is still intact, actively preventing *hox5*- mX neurons in the anterior region from innervating *hox5+* posterior targets. Similarly, in our ectopic *hox5* expression experiment, the timing mechanism is still intact, which may have led to a relatively mild bias in posterior targeting compared to anterior → posterior transplants that alter both *hox5* expression and time of axon initiation.

In future experiments, we will test this "belt-and-suspenders" hypothesis by disrupting both the *hox5*-dependent spatial mechanism and the axon outgrowth-dependent temporal mechanism. Currently, the best method we have to disrupt the temporal mechanism is heterochronic transplantation. We will carry out heterochronic transplantation into *hox5* triple mutant hosts, which will eliminate the *hox5* mechanism

that is presumably preventing late-arriving *hox5-* neurons from innervating *hox5+* posterior targets. While heterochronic transplantation of an mX neuron from young anterior WT donor → old anterior WT host leads to mild bias towards posterior targets, we predict that heterochronic transplantation of an mX neuron from young anterior WT donor → old anterior *hox5* triple mutant host will lead to stronger bias towards posterior targets. Additionally, we may combine heterochronic transplantation with our *hox5* gain-of-function approach, though this experiment may be technically difficult due to low numbers of ectopic *hox5*-expressing cells. If we transplant an anterior ectopic *hox5+* mX neuron from a young donor into the anterior region of a young stage-matched WT host, we predict the bias in posterior targeting will be relatively mild, comparable to ectopic *hox5* expression alone. However, if we transplant an anterior ectopic *hox5+* mX neuron from a young donor into the anterior region of an older WT host, we predict a stronger bias towards posterior targets compared to stage-matched transplants.

In summary, we present here several novel findings to expand understanding of topographic map development. We characterize the development of the larval zebrafish vagus motor neuron topographic map and demonstrate that map development is governed by *hox5* genes expressed in posterior mX neurons, as well as delayed axon initiation in posterior mX neurons that subsequently leads to late arrival in the periphery. Future experiments will identify *hox5* targets that direct axon targeting, elucidate how axon initiation is regulated independently of cell birth, and ascertain how the *hox5*-dependent spatial mechanism and axon outgrowth-dependent temporal mechanism work together in map development.

References

Anderson, R. M., Delous, M., Bosch, J. A., Ye, L., Robertson, M. A., Hesselson, D., & Stainier, D. Y. R. (2013). Hepatocyte Growth Factor Signaling in Intrapancreatic Ductal Cells Drives Pancreatic Morphogenesis. *PLoS Genetics*, *9*(7), e1003650. https://doi.org/10.1371/journal.pgen.1003650

Andreae, L. C., Lumsden, A., & Gilthorpe, J. D. (2009). Chick Lrrn2, a novel downstream effector of Hoxb1 and Shh, functions in the selective targeting of rhombomere 4 motor neurons. *Neural Development*, *4*, 27. https://doi.org/10.1186/1749-8104-4-27

Arenkiel, B. R., Gaufo, G. O., & Capecchi, M. R. (2003). Hoxb1 neural crest preferentially form glia of the PNS. *Developmental Dynamics : An Official Publication of the American Association of Anatomists*, *227*(3), 379–86. https://doi.org/10.1002/dvdy.10323

Barnes, A. P., Lilley, B. N., Pan, Y. A., Plummer, L. J., Powell, A. W., Raines, A. N., … Polleux, F. (2007). LKB1 and SAD Kinases Define a Pathway Required for the Polarization of Cortical Neurons. *Cell*, *129*(3), 549–563. https://doi.org/10.1016/j.cell.2007.03.025

Bechara, A., Laumonnerie, C., Vilain, N., Kratochwil, C. F., Cankovic, V., Maiorano, N. A., … Rijli, F. M. (2015). Hoxa2 Selects Barrelette Neuron Identity and Connectivity in the Mouse Somatosensory Brainstem. *Cell Reports*, *13*(4), 783–797. https://doi.org/10.1016/j.celrep.2015.09.031

Bell, E., Wingate, R., & Lumsden, A. (1999). Homeotic transformation of rhombomere identity after localized Hoxb1 misexpression. *Science*, *284*(5423), 2168–2171.

Bieger, D., & Hopkins, D. A. (1987). Viscerotopic representation of the upper alimentary tract in the medulla oblongata in the rat: The nucleus ambiguus. *Journal of Comparative Neurology*, *262*(4), 546–562. https://doi.org/10.1002/cne.902620408

Blumenfeld, H. (2010). *Neuroanatomy through Clinical Cases*. *Copyright © 2010 by Sinauer Associates, Inc.* https://doi.org/10.1017/CBO9781107415324.004

Boylan, J. F., & Gudas, L. J. (1991). Overexpression of the cellular retinoic acid binding protein-I (CRABP-I) results in a reduction in differentiation-specific gene expression in F9 teratocarcinoma cells. *The Journal of Cell Biology*, *112*(5), 965–79. Retrieved from http://www.ncbi.nlm.nih.gov/pubmed/1847931

Brown, N. L., Patel, S., Brzezinski, J., & Glaser, T. (2001). Math5 is required for retinal ganglion cell and optic nerve formation. *Development*, *128*, 2497–2508.

Bruce, A. E. E., Oates, A. C., Prince, V. E., & Ho, R. K. (2001). Additional hox clusters in the zebrafish: Divergent expression patterns belie equivalent activities of duplicate hoxB5 genes. *Evolution and Development*, *3*(3), 127–144. https://doi.org/10.1046/j.1525-142X.2001.003003127.x

Cambronero, F., & Puelles, L. (2000). Rostrocaudal nuclear relationships in the avian medulla oblongata: A fate map with quail chick chimeras. *The Journal of Comparative Neurology*, *427*(4), 522–545. https://doi.org/10.1002/1096-9861(20001127)427:4<522::AID-CNE3>3.0.CO;2-Y

Cang, J., & Feldheim, D. A. (2013). Developmental Mechanisms of Topographic Map

Formation and Alignment. *Annu. Rev. Neurosci*, *36*, 51–77. https://doi.org/10.1146/annurev-neuro-062012-170341
Caton, A., Hacker, A., Naeem, A., Livet, J., Maina, F., Bladt, F., … Guthrie, S. (2000). The branchial arches and HGF are growth-promoting and chemoattractant for cranial motor axons. *Development (Cambridge, England)*, *127*(8), 1751–1766.
Chandrasekhar, A. (2004). Turning heads: development of vertebrate branchiomotor neurons. *Dev Dyn*, *229*(1), 143–161. https://doi.org/10.1002/dvdy.10444
Chen, S., Chen, J., Shi, H., Wei, M., Castaneda-Castellanos, D. R., Bultje, R. S., … Shi, S. H. (2013). Regulation of Microtubule Stability and Organization by Mammalian Par3 in Specifying Neuronal Polarity. *Developmental Cell*, *24*(1), 26–40. https://doi.org/10.1016/j.devcel.2012.11.014
Cheng, H. J., Nakamoto, M., Bergemann, A. D., & Flanagan, J. G. (1995). Complementary gradients in expression and binding of ELF-1 and Mek4 in development of the topographic retinotectal projection map. *Cell*, *82*(3), 371–381. https://doi.org/10.1016/0092-8674(95)90426-3
Connor, R. J., Menzel, P., & Pasquale, E. B. (1998). Expression and tyrosine phosphorylation of Eph receptors suggest multiple mechanisms in patterning of the visual system. *Developmental Biology*, *193*(1), 21–35. https://doi.org/10.1006/dbio.1997.8786
Cox, J., Lamora, A., Johnson, S., & Voigt, M. (2011). Diverse mechanisms for assembly of branchiomeric nerves. *Dev Biol*, *357*(2), 305–317. https://doi.org/10.1016/j.ydbio.2011.06.044
Dasen, J. S., De Camilli, A., Wang, B., Tucker, P. W., & Jessell, T. M. (2008). Hox Repertoires for Motor Neuron Diversity and Connectivity Gated by a Single Accessory Factor, FoxP1. *Cell*, *134*(2), 304–316. https://doi.org/10.1016/j.cell.2008.06.019
Dasen, J. S., Liu, J.-P., & Jessell, T. M. (2003). Motor neuron columnar fate imposed by sequential phases of Hox-c activity. *Nature*, *425*(6961), 926–933. https://doi.org/10.1038/nature02051
Dasen, J. S., Tice, B. C., Brenner-Morton, S., & Jessell, T. M. (2005). A Hox regulatory network establishes motor neuron pool identity and target-muscle connectivity. *Cell*, *123*(3), 477–491. https://doi.org/10.1016/j.cell.2005.09.009
Davey, C. F., Mathewson, A. W., & Moens, C. B. (2016). PCP Signaling between Migrating Neurons and their Planar-Polarized Neuroepithelial Environment Controls Filopodial Dynamics and Directional Migration. *PLoS Genetics*, *12*(3). https://doi.org/10.1371/journal.pgen.1005934
Davison, J. M., Akitake, C. M., Goll, M. G., Rhee, J. M., Gosse, N., Baier, H., … Parsons, M. J. (2007). Transactivation from Gal4-VP16 transgenic insertions for tissue-specific cell labeling and ablation in zebrafish. *Developmental Biology*, *304*(2), 811–24. https://doi.org/10.1016/j.ydbio.2007.01.033
Delva, L., Bastie, J. N., Rochette-Egly, C., Kraïba, R., Balitrand, N., Despouy, G., … Chomienne, C. (1999). Physical and functional interactions between cellular retinoic acid binding protein II and the retinoic acid-dependent nuclear complex. *Molecular and Cellular Biology*, *19*(10), 7158–67. Retrieved from

http://www.ncbi.nlm.nih.gov/pubmed/10490651
Demireva, E. Y., Shapiro, L. S., Jessell, T. M., & Zampieri, N. (2011). Motor Neuron Position and Topographic Order Imposed by β- and {γ-Catenin} Activities. *Cell*, *147*(3), 641–652. https://doi.org/10.1016/j.cell.2011.09.037
Dotti, C. G., Sullivan, C. A., & Banker, G. A. (1988). The establishment of polarity by hippocampal neurons in culture. *The Journal of Neuroscience : The Official Journal of the Society for Neuroscience*, *8*(4), 1454–68. Retrieved from http://www.ncbi.nlm.nih.gov/pubmed/3282038
Drescher, U., Kremoser, C., Handwerker, C., Löschinger, J., Noda, M., & Bonhoeffer, F. (1995). In vitro guidance of retinal ganglion cell axons by RAGS, a 25 kDa tectal protein related to ligands for Eph receptor tyrosine kinases. *Cell*, *82*(3), 359–370. https://doi.org/10.1016/0092-8674(95)90425-5
Duan, X., Krishnaswamy, A., De la Huerta, I., & Sanes, J. R. (2014). Type II Cadherins Guide Assembly of a Direction-Selective Retinal Circuit. *Cell*, *158*(4), 793–807. https://doi.org/10.1016/j.cell.2014.06.047
Dyer, C., Linker, C., Graham, A., & Knight, R. (2014). Specification of sensory neurons occurs through diverse developmental programs functioning in the brain and spinal cord. *Developmental Dynamics*, *243*(11), 1429–1439. https://doi.org/10.1002/dvdy.24184
Eerdunfu, Ihara, N., Ligao, B., Ikegaya, Y., & Takeuchi, H. (2017). Differential timing of neurogenesis underlies dorsal-ventral topographic projection of olfactory sensory neurons. *Neural Development*, *12*(1), 2. https://doi.org/10.1186/s13064-017-0079-0
Eisen, J. (1991). Determination of primary motoneuron identity in developing zebrafish embryos. *Science*, *252*(5005), 569–572.
Erman, A. B., Kejner, A. E., Hogikyan, N. D., & Feldman, E. L. (2009). Disorders of cranial nerves IX and X. *Seminars in Neurology*. https://doi.org/10.1055/s-0028-1124027
Erzurumlu, R. S., Murakami, Y., & Rijli, F. M. (2010). Mapping the face in the somatosensory brainstem. *Nature Reviews Neuroscience*, *11*(4), 252–263. https://doi.org/10.1038/nrn2804
Feldheim, D. A., Kim, Y.-I., Bergemann, A. D., Frisé, J., Barbacid, M., & Flanagan, J. G. (2000). Genetic Analysis of Ephrin-A2 and Ephrin-A5 Shows Their Requirement in Multiple Aspects of Retinocollicular Mapping. *Neuron*, *25*, 563–574. https://doi.org/10.1016/S0896-6273(00)81060-0
Frisen, J., Yates, P. A., McLaughlin, T., Friedman, G. C., O'Leary, D. D. M., & Barbacid, M. (1998). Ephrin-A5 (AL-1/RAGS) is essential for proper retinal axon guidance and topographic mapping in the mammalian visual system. *Neuron*, *20*(2), 235–243. https://doi.org/10.1016/S0896-6273(00)80452-3
Galiano, M. R., Jha, S., Ho, T. S.-Y., Zhang, C., Ogawa, Y., Chang, K.-J., … Rasband, M. N. (2012). A Distal Axonal Cytoskeleton Forms an Intra-Axonal Boundary that Controls Axon Initial Segment Assembly. *Cell*, *149*(5), 1125–1139. https://doi.org/10.1016/j.cell.2012.03.039
Geisen, M. J., Di Meglio, T., Pasqualetti, M., Ducret, S., Brunet, J. F., Chedotal, A., & Rijli, F. M. (2008). Hox paralog group 2 genes control the migration of mouse

pontine neurons through slit-Robo signaling. *PLoS Biology*, *6*(6), 1178–1194. https://doi.org/10.1371/journal.pbio.0060142
Gilland, E., & Baker, R. (2005). Evolutionary patterns of cranial nerve efferent nuclei in vertebrates. In *Brain, Behavior and Evolution* (Vol. 66, pp. 234–254). https://doi.org/10.1159/000088128
Grant, P., & Moens, C. (2010). The neuroepithelial basement membrane serves as a boundary and a substrate for neuron migration in the zebrafish hindbrain. *Neural Dev*, *5*, 9. https://doi.org/10.1186/1749-8104-5-9
Guthrie, S. (2007). Patterning and axon guidance of cranial motor neurons. *Nat Rev Neurosci*, *8*(11), 859–871. https://doi.org/10.1038/nrn2254
Guthrie, S., & Lumsden, A. (1992). Motor neuron pathfinding following rhombomere reversals in the chick embryo hindbrain. *Development*, *114*(3), 663–673.
Hatanaka, Y., & Yamauchi, K. (2013). Excitatory cortical neurons with multipolar shape establish neuronal polarity by forming a tangentially oriented axon in the intermediate zone. *Cerebral Cortex*, *23*(1), 105–113. https://doi.org/10.1093/cercor/bhr383
Hedstrom, K. L., Ogawa, Y., & Rasband, M. N. (2008). AnkyrinG is required for maintenance of the axon initial segment and neuronal polarity. *The Journal of Cell Biology*, *183*(4), 635–640. https://doi.org/10.1083/jcb.200806112
Higashijima, S., Hotta, Y., & Okamoto, H. (2000). Visualization of cranial motor neurons in live transgenic zebrafish expressing green fluorescent protein under the control of the islet-1 promoter/enhancer. *J Neurosci*, *20*(1), 206–218.
Hilde, K. L., Levine, A. J., Hinckley, C. A., Hayashi, M., Montgomery, J. M., Gullo, M., … Pfaff, S. L. (2016). Satb2 Is Required for the Development of a Spinal Exteroceptive Microcircuit that Modulates Limb Position. *Neuron*, *91*(4), 763–776. https://doi.org/10.1016/j.neuron.2016.07.014
Hindges, R., McLaughlin, T., Genoud, N., Henkemeyer, M., & O'Leary, D. D. M. (2002). EphB forward signaling controls directional branch extension and arborization required for dorsal-ventral retinotopic mapping. *Neuron*, *35*(3), 475–487. https://doi.org/10.1016/S0896-6273(02)00799-7
Holt, C. E. (1984). Does timing of axon outgrowth influence initial retinotectal topography in Xenopus? *The Journal of Neuroscience : The Official Journal of the Society for Neuroscience*, *4*(4), 1130–1152.
Holzschuh, J., Wada, N., Wada, C., Schaffer, A., Javidan, Y., Tallafuß, A., … Schilling, T. F. (2005). Requirements for endoderm and {BMP} signaling in sensory neurogenesis in zebrafish. *Development*, *132*(16), 3731–3742. https://doi.org/10.1242/dev.01936
Hortopan, G. A., & Baraban, S. C. (2011). Aberrant expression of genes necessary for neuronal development and notch signaling in an epileptic mind bomb zebrafish. *Developmental Dynamics*, *240*(8), 1964–1976. https://doi.org/10.1002/dvdy.22680
Imai, T., Sakano, H., & Vosshall, L. B. (2010). Topographic mapping--the olfactory system. *Cold Spring Harbor Perspectives in Biology*. https://doi.org/10.1101/cshperspect.a001776
Jing, Y., Waxman, S., & Mira-y-Lopez, R. (1997). The cellular retinoic acid binding

protein II is a positive regulator of retinoic acid signaling in breast cancer cells. *Cancer Research*, *57*(9), 1668–72. Retrieved from http://www.ncbi.nlm.nih.gov/pubmed/9135005

Kam, R. K. T., Shi, W., Chan, S. O., Chen, Y., Xu, G., Lau, C. B.-S., … Zhao, H. (2013). Dhrs3 Protein Attenuates Retinoic Acid Signaling and Is Required for Early Embryonic Patterning. *Journal of Biological Chemistry*, *288*(44), 31477–31487. https://doi.org/10.1074/jbc.M113.514984

Kania, A., & Jessell, T. M. (2003). Topographic motor projections in the limb imposed by {LIM} homeodomain protein regulation of {ephrin-A:EphA} interactions., *38*(4), 581–596.

Kapitein, L. C., & Hoogenraad, C. C. (2015). Building the Neuronal Microtubule Cytoskeleton. *Neuron*. https://doi.org/10.1016/j.neuron.2015.05.046

Karmakar, K., Narita, Y., Fadok, J., Ducret, S., Loche, A., Kitazawa, T., … Rijli, F. M. (2017). Hox2 Genes Are Required for Tonotopic Map Precision and Sound Discrimination in the Mouse Auditory Brainstem. *Cell Reports*, *18*(1), 185–197. https://doi.org/10.1016/j.celrep.2016.12.021

Karpinski, B., Maynard, T., Fralish, M., Nuwayhid, S., Zohn, I., Moody, S., & A., L. (2014). Dysphagia and disrupted cranial nerve development in a mouse model of {DiGeorge} (22q11) deletion syndrome. *Dis Model Mech*, *7*(2), 245–257. https://doi.org/10.1242/dmm.012484

Kemp, H. A., Carmany-Rampey, A., & Moens, C. (2009). Generating chimeric zebrafish embryos by transplantation. *Journal of Visualized Experiments : JoVE*, (29). https://doi.org/10.3791/1394

Kimmel, C. B., Ballard, W. W., Kimmel, S. R., Ullmann, B., & Schilling, T. F. (1995). Stages of embryonic development of the zebrafish. *Dev Dyn*, *203*(3), 253–310. https://doi.org/10.1002/aja.1002030302

Kimura, Y., Hisano, Y., Kawahara, A., & Higashijima, S. (2014). Efficient generation of knock-in transgenic zebrafish carrying reporter/driver genes by CRISPR/Cas9-mediated genome engineering. *Scientific Reports*, *4*, 6545. https://doi.org/10.1038/srep06545

Kishi, M., Pan, Y. A., Crump, J. G., & Sanes, J. R. (2005). Mammalian SAD kinases are required for neuronal polarization. *Science*, *307*(5711), 929–932. https://doi.org/10.1126/science.1107403

Kramer, E. R., Knott, L., Su, F., Dessaud, E., Krull, C. E., Helmbacher, F., & Klein, R. (2006). Cooperation between GDNF/Ret and ephrinA/EphA4 Signals for Motor-Axon Pathway Selection in the Limb. *Neuron*, *50*(1), 35–47. https://doi.org/10.1016/j.neuron.2006.02.020

Krumlauf, R. (2016). Hox Genes and the Hindbrain. A Study in Segments. In *Current Topics in Developmental Biology* (Vol. 116, pp. 581–596). https://doi.org/10.1016/bs.ctdb.2015.12.011

Kudoh, T., Tsang, M., Hukriede, N. A., Chen, X., Dedekian, M., Clarke, C. J., … Dawid, I. B. (2001). A gene expression screen in zebrafish embryogenesis. *Genome Research*, *11*(12), 1979–1987. https://doi.org/10.1101/gr.209601

Kuijpers, M., Van de Willige, D., Freal, A., Chazeau, A., Franker, M. A., Hofenk, J., …

Hoogenraad, C. C. (2016). Dynein Regulator NDEL1 Controls Polarized Cargo Transport at the Axon Initial Segment. *Neuron*, *89*(3), 461–471. https://doi.org/10.1016/j.neuron.2016.01.022

Kulkarni, A., Ertekin, D., Lee, C. H., & Hummel, T. (2016). Birth order dependent growth cone segregation determines synaptic layer identity in the Drosophila visual system. *eLife*, *5*(MARCH2016). https://doi.org/10.7554/eLife.13715

Kwan, K. M., Fujimoto, E., Grabher, C., Mangum, B. D., Hardy, M. E., Campbell, D. S., … Chien, C.-B. (2007). The Tol2kit: a multisite gateway-based construction kit for Tol2 transposon transgenesis constructs. *Developmental Dynamics : An Official Publication of the American Association of Anatomists*, *236*(11), 3088–99. https://doi.org/10.1002/dvdy.21343

LaMantia, A. S., Moody, S. A., Maynard, T. M., Karpinski, B. A., Zohn, I. E., Mendelowitz, D., … Popratiloff, A. (2016). Hard to swallow: Developmental biological insights into pediatric dysphagia. *Developmental Biology*. https://doi.org/10.1016/j.ydbio.2015.09.024

Landmesser, L. (1978). The development of motor projection patterns in the chick hind limb. *The Journal of Physiology*, *284*, 391–414. Retrieved from http://www.pubmedcentral.nih.gov/articlerender.fcgi?artid=1282827&tool=pmcentrez&rendertype=abstract

Lee, J.-A., Anholt, R. R. H., & Cole, G. J. (2008). Olfactomedin-2 mediates development of the anterior central nervous system and head structures in zebrafish. *Mechanisms of Development*, *125*(1–2), 167–181. https://doi.org/10.1016/j.mod.2007.09.009

Levine, A. J., Lewallen, K. A., & Pfaff, S. L. (2012). Spatial organization of cortical and spinal neurons controlling motor behavior. *Current Opinion in Neurobiology*. https://doi.org/10.1016/j.conb.2012.07.002

Liu, R.-Z., Sharma, M. K., Sun, Q., Thisse, C., Thisse, B., Denovan-Wright, E. M., & Wright, J. M. (2005). Retention of the duplicated cellular retinoic acid-binding protein 1 genes (crabp1a and crabp1b) in the zebrafish genome by subfunctionalization of tissue-specific expression. *FEBS Journal*, *272*(14), 3561–3571. https://doi.org/10.1111/j.1742-4658.2005.04775.x

Lorenzo, D. N., Badea, A., Davis, J., Hostettler, J., He, J., Zhong, G., … Bennett, V. (2014). A PIK3C3–Ankyrin-B–Dynactin pathway promotes axonal growth and multiorganelle transport. *The Journal of Cell Biology*, *207*(6), 735–752. https://doi.org/10.1083/jcb.201407063

Luo, L., & Flanagan, J. G. (2007). Development of continuous and discrete neural maps. *Neuron*, *56*(2), 284–300. https://doi.org/10.1016/j.neuron.2007.10.014

Luria, V., Krawchuk, D., Jessell, T. M., Laufer, E., & Kania, A. (2008). Specification of Motor Axon Trajectory by Ephrin-B:EphB Signaling: Symmetrical Control of Axonal Patterning in the Developing Limb. *Neuron*, *60*(6), 1039–1053. https://doi.org/10.1016/j.neuron.2008.11.011

Mann, F., Ray, S., Harris, W. A., & Holt, C. E. (2002). Topographic mapping in dorsoventral axis of the Xenopus retinotectal system depends on signaling through ephrin-B ligands. *Neuron*, *35*(3), 461–473. https://doi.org/10.1016/S0896-

6273(02)00786-9
Marcus, R. C., Gale, N. W., Morrison, M. E., Mason, C. A., & Yancopoulos, G. D. (1996). *Eph Family Receptors and Their Ligands Distribute in Opposing Gradients in the Developing Mouse Retina*. *Developmental Biology* (Vol. 180). https://doi.org/10.1006/dbio.1996.0347
Matsuo, K., & Palmer, J. B. (2008). Anatomy and Physiology of Feeding and Swallowing: Normal and Abnormal. *Physical Medicine and Rehabilitation Clinics of North America*, *19*(4), 691–707. https://doi.org/10.1016/j.pmr.2008.06.001
McClintock, J. M., Carlson, R., Mann, D. M., & Prince, V. E. (2001). Consequences of Hox gene duplication in the vertebrates: an investigation of the zebrafish Hox paralogue group 1 genes. *Development (Cambridge, England)*, *128*(13), 2471–84. Retrieved from http://www.ncbi.nlm.nih.gov/pubmed/11493564
Moens, C., & Prince, V. (2002). Constructing the hindbrain: insights from the zebrafish. *Dev Dyn*, *224*(1), 1–17. https://doi.org/10.1002/dvdy.10086
Morgan, J. L., Dhingra, A., Vardi, N., & Wong, R. O. (2006). Axons and dendrites originate from neuroepithelial-like processes of retinal bipolar cells. *Nat Neurosci*, *9*(1), 85–92. https://doi.org/10.1038/nn1615
Morita, Y., & Finger, T. E. (1985). Topographic and laminar organization of the vagal gustatory system in the goldfish, carassius auratus. *Journal of Comparative Neurology*, *238*(2), 187–201. https://doi.org/10.1002/cne.902380206
Nagelberg, D., Wang, J., Su, R., Torres-Vázquez, J., Targoff, K. L., Poss, K. D., & Knaut, H. (2015). Origin, specification, and plasticity of the great vessels of the heart. *Current Biology*, *25*(16), 2099–2110. https://doi.org/10.1016/j.cub.2015.06.076
Nakamoto, M., Cheng, H. J., Friedman, G. C., McLaughlin, T., Hansen, M. J., Yoon, C. H., … Flanagan, J. G. (1996). Topographically specific effects of ELF-1 on retinal axon guidance in vitro and retinal axon mapping in vivo. *Cell*, *86*(5), 755–766. https://doi.org/10.1016/S0092-8674(00)80150-6
Namba, T., Kibe, Y., Funahashi, Y., Nakamuta, S., Takano, T., Ueno, T., … Kaibuchi, K. (2014). Pioneering axons regulate neuronal polarization in the developing cerebral cortex. *Neuron*, *81*(4), 814–829. https://doi.org/10.1016/j.neuron.2013.12.015
Nern, A., Zhu, Y., & Zipursky, S. L. (2008). Local N-Cadherin Interactions Mediate Distinct Steps in the Targeting of Lamina Neurons. *Neuron*, *58*(1), 34–41. https://doi.org/10.1016/j.neuron.2008.03.022
Ninov, N., Borius, M., & Stainier, D. Y. R. (2012). Different levels of Notch signaling regulate quiescence, renewal and differentiation in pancreatic endocrine progenitors. *Development*, *139*(9), 1557–1567. https://doi.org/10.1242/dev.076000
Noctor, S. C., Martínez-Cerdeño, V., Ivic, L., & Kriegstein, A. R. (2004). Cortical neurons arise in symmetric and asymmetric division zones and migrate through specific phases. *Nature Neuroscience*, *7*(2), 136–144. https://doi.org/10.1038/nn1172
Ohata, S., Kinoshita, S., Aoki, R., Tanaka, H., Wada, H., S., T.-K., … Okamoto, H. (2009). Neuroepithelial cells require fucosylated glycans to guide the migration of vagus motor neuron progenitors in the developing zebrafish hindbrain.

Development, *136*(10), 1653–1663. https://doi.org/10.1242/dev.033290
Olsson, C., Holmberg, A., & Holmgren, S. (2008). Development of enteric and vagal innervation of the zebrafish {(Danio} rerio) gut. *J Comp Neurol*, *508*(5), 756–770. https://doi.org/10.1002/cne.21705
Osterhout, J. A., El-Danaf, R. N., Nguyen, P. L., & Huberman, A. D. (2014). Birthdate and outgrowth timing predict cellular mechanisms of axon target matching in the developing visual pathway. *Cell Reports*, *8*(4), 1006–17. https://doi.org/10.1016/j.celrep.2014.06.063
Oury, F., Murakami, Y., Renaud, J., Pasqualetti, M., Charnay, P., Ren, S., & Rijli, F. M. (2006). Hoxa2- and Rhombomere-Dependent Development of the Mouse Facial Somatosensory Map. *Science*, (September), 1408–1413. https://doi.org/10.1126/science.1130042
Paré, A. C., Vichas, A., Fincher, C. T., Mirman, Z., Farrell, D. L., Mainieri, A., & Zallen, J. A. (2014). A positional Toll receptor code directs convergent extension in Drosophila. *Nature*, *515*(7528), 523–7. https://doi.org/10.1038/nature13953
Parker, H. J., Bronner, M. E., & Krumlauf, R. (2016). The vertebrate *Hox* gene regulatory network for hindbrain segmentation: Evolution and diversification. *BioEssays*, *38*(6), 526–538. https://doi.org/10.1002/bies.201600010
Peris, B., Gonzalez-Granero, S., Ballester-Lurbe, B., García-Verdugo, J.-M., Pérez-Roger, I., Guerri, C., … Guasch, R. M. (2012). Neuronal polarization is impaired in mice lacking RhoE expression. *Journal of Neurochemistry*, *121*(6), 903–14. https://doi.org/10.1111/j.1471-4159.2012.07733.x
Petrovic, M., & Hummel, T. (2008). Temporal identity in axonal target layer recognition. *Nature*, *456*(7223), 800–803. https://doi.org/10.1038/nature07407
Pfeiffenberger, C., Yamada, J., & Feldheim, D. A. (2006). Ephrin-As and patterned retinal activity act together in the development of topographic maps in the primary visual system. *The Journal of Neuroscience : The Official Journal of the Society for Neuroscience*, *26*(50), 12873–84. https://doi.org/10.1523/JNEUROSCI.3595-06.2006
Philippidou, P., & Dasen, J. S. (2013). Hox Genes: Choreographers in Neural Development, Architects of Circuit Organization. *Neuron*. https://doi.org/10.1016/j.neuron.2013.09.020
Poliak, S., Morales, D., Croteau, L.-P., Krawchuk, D., Palmesino, E., Morton, S., … Kania, A. (2015). Synergistic integration of Netrin and ephrin axon guidance signals by spinal motor neurons Sebastian. *eLife*, *4*(December), 1–26. https://doi.org/10.1017/CBO9781107415324.004
Polleux, F., & Snider, W. (2010). Initiating and growing an axon. *Cold Spring Harbor Perspectives in Biology*. https://doi.org/10.1101/cshperspect.a001925
Prince, V. E., Joly, L., Ekker, M., & Ho, R. K. (1998). Zebrafish hox genes: genomic organization and modified colinear expression patterns in the trunk. *Development*, *125*(3), 407–420.
Prince, V. E., Moens, C. B., Kimmel, C. B., & Ho, R. K. (1998). Zebrafish hox genes: expression in the hindbrain region of wild-type and mutants of the segmentation gene, valentino. *Development (Cambridge, England)*, *125*(3), 393–406.

Qu, F., Lorenzo, D. N., King, S. J., Brooks, R., Bear, J. E., & Bennett, V. (2016). Ankyrin-B is a PI3P effector that promotes polarized α5β1-integrin recycling via recruiting RabGAP1L to early endosomes. *eLife*, *5*. https://doi.org/10.7554/eLife.20417

Randlett, O., Poggi, L., Zolessi, F. R., & Harris, W. A. (2011). The Oriented Emergence of Axons from Retinal Ganglion Cells Is Directed by Laminin Contact In Vivo. *Neuron*, *70*(2), 266–280. https://doi.org/10.1016/j.neuron.2011.03.013

Rathelot, J.-A., & Strick, P. L. (2006). Muscle representation in the macaque motor cortex: An anatomical perspective. *Proceedings of the National Academy of Sciences*, *103*(21), 8257–8262. https://doi.org/10.1073/pnas.0602933103

Sasaki, S., Shionoya, A., Ishida, M., Gambello, M. J., Yingling, J., Wynshaw-Boris, A., & Hirotsune, S. (2000). A LIS1/NUDEL/cytoplasmic dynein heavy chain complex in the developing and adult nervous system. *Neuron*, *28*(3), 681–696. https://doi.org/10.1016/S0896-6273(00)00146-X

Schilling, T., & Kimmel, C. (1997). Musculoskeletal patterning in the pharyngeal segments of the zebrafish embryo. *Development*, *124*(15), 2945–2960.

Shah, A. N., Davey, C. F., Whitebirch, A. C., Miller, A. C., & Moens, C. B. (2015). Rapid reverse genetic screening using CRISPR in zebrafish. *Nature Methods*, *12*(6), 535–540. https://doi.org/10.1038/nmeth.3360

Shelly, M., Cancedda, L., Heilshorn, S., Sumbre, G., & Poo, M. ming. (2007). LKB1/STRAD Promotes Axon Initiation During Neuronal Polarization. *Cell*, *129*(3), 565–577. https://doi.org/10.1016/j.cell.2007.04.012

Shelly, M., Cancedda, L., Lim, B. K., Popescu, A. T., Cheng, P. lin, Gao, H., & Poo, M. ming. (2011). Semaphorin3A regulates neuronal polarization by suppressing axon formation and promoting dendrite growth. *Neuron*, *71*(3), 433–446. https://doi.org/10.1016/j.neuron.2011.06.041

Shi, S. H., Jan, L. Y., & Jan, Y. N. (2003). Hippocampal neuronal polarity specified by spatially localized mPar3/mPar6 and PI 3-kinase activity. *Cell*. https://doi.org/10.1016/S0092-8674(02)01249-7

Sittaramane, V., & Chandrasekhar, A. (2008). *Expression of unconventional myosin genes during neuronal development in zebrafish*. *Gene Expression Patterns* (Vol. 8). https://doi.org/10.1016/j.gep.2007.10.010

Sperber, S. M., & Dawid, I. B. (2008). barx1 is necessary for ectomesenchyme proliferation and osteochondroprogenitor condensation in the zebrafish pharyngeal arches. *Developmental Biology*, *321*(1), 101–10. https://doi.org/10.1016/j.ydbio.2008.06.004

Sperry, R. W. (1963). Chemoaffinity in the orderly growth of nerve fiber patterns and connections. *Proceedings of the National Academy of Sciences of the United States of America*, *50*, 703–10. Retrieved from http://www.ncbi.nlm.nih.gov/pubmed/14077501

Takeuchi, H., Inokuchi, K., Aoki, M., Suto, F., Tsuboi, A., Matsuda, I., … Sakano, H. (2010). Sequential arrival and graded secretion of Sema3F by olfactory neuron axons specify map topography at the bulb. *Cell*, *141*(6), 1056–1067. https://doi.org/10.1016/j.cell.2010.04.041

Thisse, B., Pflumio, S., Fürthauer, M., Loppin, B., Heyer, V., Degrave, A., … Thisse, C. (2001). Expression of the zebrafish genome during embryogenesis. https://doi.org/cb646

Thisse, B., & Thisse, C. (2004). Fast Release Clones: A High Throughput Expression Analysis. *ZFIN Direct Data Submission*.

Thisse, C., & Thisse, B. (2008). High-resolution in situ hybridization to whole-mount zebrafish embryos. *Nature Protocols*, *3*(1), 59–69. https://doi.org/10.1038/nprot.2007.514

Tomás-Roca, L., Corral-San-Miguel, R., Aroca, P., Puelles, L., & Marín, F. (2016). Crypto-rhombomeres of the mouse medulla oblongata, defined by molecular and morphological features. *Brain Structure and Function*, *221*(2), 815–838. https://doi.org/10.1007/s00429-014-0938-y

Triplett, J. W. (2014). Molecular guidance of retinotopic map development in the midbrain. *Current Opinion in Neurobiology*. https://doi.org/10.1016/j.conb.2013.07.006

Triplett, J. W., & Feldheim, D. A. (2012). Eph and ephrin signaling in the formation of topographic maps. *Seminars in Cell and Developmental Biology*. https://doi.org/10.1016/j.semcdb.2011.10.026

Triplett, J. W., Pfeiffenberger, C., Yamada, J., Stafford, B. K., Sweeney, N. T., Litke, a. M., … Feldheim, D. a. (2011). Competition is a driving force in topographic mapping. *Proceedings of the National Academy of Sciences*, *108*(47), 19060–19065. https://doi.org/10.1073/pnas.1102834108

Tsuchida, T., Ensini, M., Morton, S. B., Baldassare, M., Edlund, T., Jessell, T. M., & Pfaff, S. L. (1994). Topographic organization of embryonic motor neurons defined by expression of LIM homeobox genes. *Cell*, *79*(6), 957–970. https://doi.org/10.1016/0092-8674(94)90027-2

van Beuningen, S. F. B., & Hoogenraad, C. C. (2016). Neuronal polarity: Remodeling microtubule organization. *Current Opinion in Neurobiology*. https://doi.org/10.1016/j.conb.2016.02.003

Van Beuningen, S. F. B., Will, L., Harterink, M., Chazeau, A., Van Battum, E. Y., Frias, C. P., … Hoogenraad, C. C. (2015). TRIM46 Controls Neuronal Polarity and Axon Specification by Driving the Formation of Parallel Microtubule Arrays. *Neuron*, *88*(6), 1208–1226. https://doi.org/10.1016/j.neuron.2015.11.012

Van Ryswyk, L., Simonson, L., & Eisen, J. S. (2014). The Role of inab in Axon Morphology of an Identified Zebrafish Motoneuron. *PLoS ONE*, *9*(2), e88631. https://doi.org/10.1371/journal.pone.0088631

Wang, F., Wolfson, S., Gharib, A., & Sagasti, A. (2012). LAR Receptor Tyrosine Phosphatases and HSPGs Guide Peripheral Sensory Axons to the Skin. *Current Biology*, *22*(5), 373–382. https://doi.org/10.1016/j.cub.2012.01.040

Wang, J., Cao, J., Dickson, A. L., & Poss, K. D. (2015). Epicardial regeneration is guided by cardiac outflow tract and Hedgehog signalling. *Nature*, *522*(7555), 226–30. https://doi.org/10.1038/nature14325

Westerfield, M. (2000). The Zebrafish Book. *Eugene*, University of Oregon Press.

Witte, H., Neukirchen, D., & Bradke, F. (2008). Microtubule stabilization specifies initial

neuronal polarization. *Journal of Cell Biology*, *180*(3), 619–632. https://doi.org/10.1083/jcb.200707042

Wiweger, M. I., Zhao, Z., van Merkesteyn, R. J. P., Roehl, H. H., & Hogendoorn, P. C. W. (2012). HSPG-Deficient Zebrafish Uncovers Dental Aspect of Multiple Osteochondromas. *PLoS ONE*, *7*(1), e29734. https://doi.org/10.1371/journal.pone.0029734

Won, J. Y., Nam, E.-C., Yoo, S. J., Kwon, H. J., Um, S. J., Han, H. S., … Kim, S. Y. (2004). The effect of cellular retinoic acid binding protein-I expression on the CYP26-mediated catabolism of all-trans retinoic acid and cell proliferation in head and neck squamous cell carcinoma. *Metabolism: Clinical and Experimental*, *53*(8), 1007–12. Retrieved from http://www.ncbi.nlm.nih.gov/pubmed/15281009

Yang, T., Yin, W., Derevyanny, V. D., Moore, L. A., & Longo, F. M. (2005). Identification of an ectodomain within the LAR protein tyrosine phosphatase receptor that binds homophilically and activates signalling pathways promoting neurite outgrowth. *The European Journal of Neuroscience*, *22*(9), 2159–70. https://doi.org/10.1111/j.1460-9568.2005.04403.x

Yau, K. W., vanBeuningen, S. F. B., Cunha-Ferreira, I., Cloin, B. M. C., vanBattum, E. Y., Will, L., … Hoogenraad, C. C. (2014). Microtubule minus-end binding protein CAMSAP2 controls axon specification and dendrite development. *Neuron*, *82*(5), 1058–1073. https://doi.org/10.1016/j.neuron.2014.04.019

Yi, J. J., Barnes, A. P., Hand, R., Polleux, F., & Ehlers, M. D. (2010). TGF-beta Signaling Specifies Axons during Brain Development. *Cell*, *142*(1), 144–157. https://doi.org/10.1016/j.cell.2010.06.010

Yu, H.-H., Houart, C., & Moens, C. B. (2004). Cloning and embryonic expression of zebrafish neuropilin genes. *Gene Expression Patterns*, *4*(4), 371–378. https://doi.org/10.1016/j.modgep.2004.01.011

Yu, H., Sun, D., Wang, N., Wang, M., Lan, Y., Fan, W., … Zhu, X. (2015). Headless Myo10 is a regulator of microtubule stability during neuronal development. *Journal of Neurochemistry*, *135*(2), 261–273. https://doi.org/10.1111/jnc.13238

Zhang, H., Berg, J. S., Li, Z., Wang, Y., Lång, P., Sousa, A. D., … Strömblad, S. (2004). Myosin-X provides a motor-based link between integrins and the cytoskeleton. *Nature Cell Biology*, *6*(6), 523–531. https://doi.org/10.1038/ncb1136

Zigman, M., Laumann-Lipp, N., Titus, T., Postlethwait, J., & Moens, C. B. (2014). Hoxb1b controls oriented cell division, cell shape and microtubule dynamics in neural tube morphogenesis. *Development*, *141*(3), 639–649. https://doi.org/10.1242/dev.098731

Zolessi, F. R., Poggi, L., Wilkinson, C. J., Chien, C.-B., & Harris, W. a. (2006). Polarization and orientation of retinal ganglion cells in vivo. *Neural Development*, *1*(2), 2. https://doi.org/10.1186/1749-8104-1-2